nature portfolio

Peer Review File

Unveiling Electric-Field-Driven Deformation Dynamics in Metal Nanostructures

Corresponding Author: Professor Guodong Meng

This file contains all reviewer reports in order by version, followed by all author rebuttals in order by version.

Version 0:

Reviewer comments:

Reviewer #1

(Remarks to the Author)
The manuscript by Li et al. presents the deformation of metal nanotips in high electrical fields, investigated in field emission transmission electron microscope (TEM). The work is methodologically flawless and delivers results that are obviously of current relevance.
In the abstract, the authors somehow justify their submission by referring to a Nature paper without providing a citation (which, in my understanding, should not be done in an abstract). You probably mean reference 6?
The authors describe experiments on three different nanotips. I can't see from the paper why 3 nanotips need to be examined, surely one tip with a small radius and one with a large radius should be enough?
The work is based on the TEM experiments and therefore it would be good if the TEM used is briefly described (and a reference given) and there could also be a note on the microscope settings (acceleration voltage, angles, defocus, ...). The images are obviously TEM brightfield images and the stripes in the particles are probably lattice fringes (e.g. in Fig. 1)? For the TEM specimen holder, the company and the country should also be specified.
The labelling in most of the images is difficult to read as it is too small. This also applies to the mu dashes, which definitely needs to be corrected.
The authors use the term SAED images (selected area electron diffraction) for some images (Fig. 3, 11 and 12 in the supplementum), but strictly speaking these are not classical SAED images but Fourier transformations (diffractograms) of the corresponding TEM images.
Try to improve the conclusions, a clearer structure would be fine.

Reviewer #2

(Remarks to the Author)
The authors present an in situ TEM study investigating the mechanisms behind electric-field-induced structural and morphological changes of tungsten nanotips during field emission. The use of a specialized and quite uncommon TEM holder enables direct visualization of these changes, which is the major strength of the study. The experimental approach is intriguing, and the opportunity to observe such electric-field-driven phenomena in real-time offers significant value to the field. However, while the results are interesting, I find that several aspects of the interpretation, presentation, and methodological clarity require further attention before the manuscript can be considered for publication in such a high impact journal.
1. The manuscript states already in the abstract (but also later in the manuscriptthat the threshold for field-induced atom evaporation is reduced by a factor of five compared to theoretical predictions. However, it remains unclear how this factor is determined, and which reference values are used for comparison. Two of the cited studies (Golubov and Tamaki & Kuroda) also report experimental results rather than purely theoretical values, contrary to the claim in the manuscript. A clear and quantitative justification of the comparison, including the experimental conditions under which the cited value was obtained, is needed for this claim to be substantiated.
2. While the authors conclude that beam-induced heating is probably negligible under the conditions used (as supported by prior literature, e.g., Egerton, 10.1016/j.micron.2004.02.003), they do not adequately address other beam effects, such as elastic displacement interactions with tungsten nuclei (aka knock-on displacements, also see Egerton). The manuscript claims the morphology remains “essentially unchanged”, but does not clarify whether this applies to more subtle atomic-scale features, such as the distribution of dislocations, adatom motion, or local diffusion processes at edges or corners. Prior

studies (e.g., 10.1063/1.5093472; 10.1017/S1431927612014274) have shown that beam irradiation can enhance diffusion and defect mobility, especially at metallic surfaces and low-coordination sites. A deeper discussion of these possible effects is needed.
3. Key experimental parameters are missing, which limits reproducibility. Paramters like electron energy, beam current, and dose rate should be specified. Additional imaging parameters, such as illumination/imaging settings and camera model, should also be included, together with details on the processing steps applied to the images (eg. FFT filtering). It would be useful to comment on whether electric field conditions during imaging or other experimental issues may have affected image contrast or resolution (referring to the delocalization effect mentioned in line 110 which is visible in the images).
4. Beam-induced hydrocarbon contamination is a known challenge in TEM and can significantly alter surface diffusion and displacment dynamics. It is not clear whether the authors took any measures to prevent or assess contamination. How was surface cleanliness ensured prior to and during the experiments? A discussion of potential contamination effects is necessary given their possible influence on surface-mediated processes.
5. The modeling section lacks important details. It is assumed that an Embedded Atom Method (EAM) potential was used (as mentioned in the reference) in the FEcMD simulations, but the specific interatomic potentials, parameters, and their validation (especially with respect to surface energies and diffusion properties) are not described. Were the potentials tested against experimental or higher-level theoretical data for tungsten? This information is essential to assess the reliability of the simulation results.
6. The illustrations labeled as “MD model” (e.g. Figure 1j, Figure 2n or figure 3l) are not clearly explained. They do not appear to be atomistic models, but rather resemble finite element method (FEM) grids? If this is the case, this should be explicitly stated. What physical quantities are being depicted, and at which simulation parameter and time point these models correspond. The relationship between these models and the experimental observations also remains unclear.
7. Given that atomistic models have already been generated through MD simulations, the authors should consider performing multislice image simulations. This would enable a direct and quantitative comparison between experimental TEM images and simulated structures, providing stronger support for their interpretations and enhancing the overall impact and rigor of the study.
8. The authors claim (line 96) that the simulations provide deeper insight into the evolution process, but the specific insights gained are not well articulated. From the supplementary information (Figures 8–10), it seems the simulations mainly serve to rule out thermal effects. If the simulations are intended only for this purpose, that should be clarified. If they offer further structural or morphological insights, those should be clearly presented and discussed.
9. A schematic of the experimental geometry is included only in the supplementary material. Given its importance for understanding the local electric field distribution and overall setup, it should be moved to the main manuscript, preferably as part of Figure 1. This will aid readers in contextualizing the results.
10. The rationale behind the selection of emission currents and treatment times for the different tip radii appears arbitrary and inconsistent. Clarification on how these parameters were chosen and how they allow for direct comparisons between different experimental conditions and tip radii would improve clarity.

In conclusion, this manuscript addresses an interesting and timely topic with a unique experimental approach. However, to meet the standards of a high-impact journal, several issues need to be resolved, particularly regarding data interpretation, methodological transparency, and the clarity of both experimental and simulation descriptions. I recommend major revisions to address the points above.

Reviewer #3

(Remarks to the Author)
The manuscript investigates the electric-field-induced deformation of tungsten nanotips using in situ transmission electron microscopy (TEM) combined with electrical biasing and modeling. The study provides a direct observation of both surface morphological evolution and internal dislocation dynamics in metallic nanostructures under strong electric fields. The insights are of interest for understanding damage mechanisms in nanoscale field-emission-based electronic devices.
In particular, the authors identify a size-dependent field-assisted evaporation mechanism at field strengths (~10 V/nm) much lower than theoretically expected. The Integration of experiments with ED-MD-PIC simulations adds support to the physical interpretation. The conclusions have implications for nanoelectronics device reliability and design.

In the following, my point-to-point comments for improvement or clarification:

1. The manuscript does not mention the use of spherical aberration (Cs) correction in the images. As the analysis includes lattice-resolved dislocation imaging and shape evolution at the sub-nanometer scale, this raises concerns about the resolution limit and image delocalization artifacts. Delocalization seems strong in the HRTEM panels in Figs 1-4. Could the authors clarify whether any OL Cs correction was used, and if not, discuss the possible limitations of interpreting dislocations dynamics and fine surface features from their HRTEM?

2. Given the reliance on Fourier-filtered images to detect dislocations, I strongly recommend that the authors complement their experimental images with multislice image simulations. These should reproduce the conditions close to the experiment, in particular defocus values and crystallographic orientation. A comparison between simulated images of defect-free tip and tip with dislocations would help validate whether the dislocation contrast observed in the experimental FFT-filtered images is physically meaningful or could be influenced by imaging artifacts. This step would significantly strengthen the interpretation of the internal defect dynamics.

3. The estimates for electric field strength, field enhancement factors, and evaporation thresholds would benefit from a more

detailed analysis of uncertainty sources, particularly in the simulations. Moreover, did the authors consider the charging of the tip due to the electric field applied? Static charge can accumulate at the surface even in metallic nanostructures and persist after the field is switched off. They contribute to the potential seen by the beam electrons during imaging in defocus conditions, as for the HRTEM images presented here. The author should discuss about this. Here is a reference in the field that the authors could cite: doi.org/10.1039/D0NR00739K

4. The observed nucleation and annihilation of dislocations are compelling, but the authors could elaborate more on whether these processes are surface-driven or related to stress release from atom evaporation.

5. The 5-minute observation intervals may be insufficient to fully capture dislocation nucleation. The authors should comment on how this temporal granularity affects the interpretation of their dynamic processes.

6. Since the local electric field is geometry-dependent, do the authors account for changes in the enhancement factor as the tip shape evolves (especially between polyhedral and spherical stages)?

7. The extrapolation to softer metals like copper and gold is interesting, but it would be more convincing if supported by literature citations or preliminary comparative data.

8. Optional. Some elements in the Supplementary Information (e.g., the experimental setup in Suppl. Fig. 1b, simulations ruling out thermal effects) may be considered for insertion in the main text or figures for better clarity, if there is place.

9. Minor edits are recommended for clarity and grammar (e.g., repeated use of “close-to-spherical”, missing third person “s” in verbs, etc.) to enhance readability.

Version 1:

Reviewer comments:

Reviewer #1

(Remarks to the Author)
The authors of the paper ‘Unveiling Electric-Field-Deformation Dynamics in Metal Nanostructures’ have taken my suggestions for improvement on board and improved the text accordingly. There is still a problem with Figure 1, however: due to the addition of two images showing the experimental setup (which I think is very good), the slightly enlarged font size is still too small. I therefore ask the authors to ensure that the lettering is clearly legible.
I also believe that the suggestions made by the other reviewers have been well addressed and implemented.
I therefore recommend the acceptance of this very interesting paper, but please improve Figure 1 beforehand.

Reviewer #2

(Remarks to the Author)
The authors have addressed all critical concerns in a satisfactory manner. I now support publication of this manuscript in its revised form.

Reviewer #3

(Remarks to the Author)
In the revision, the authors have addressed the reviewer comments thoroughly, and the manuscript is now significantly improved in clarity, methodology, and depth of interpretation.
I appreciate the inclusion of multislice image simulations, which validate that the dislocation contrasts observed in the FFT-filtered HRTEM images are physically meaningful. The clarification and the discussion of possible resolution limits are transparent and scientifically honest. The authors also expanded the discussion on the evolution of the field enhancement factor, improved figure quality and annotation, and integrated data from the Supplementary Information into the main text. These changes enhance the manuscript’s readability and coherence.
Overall, the revised version now presents a clear and compelling story supported by quantitative analysis and well-controlled in situ experiments.
I am satisfied that my previous comments, as well as those from the other reviewers, have been addressed.
I support publication of the manuscript in its present form.
Note: There is a minor typo in ref 56 in manuscript file and ref. 2 in Supporting Information. Please check.

REVIEWER COMMENTS

Report of Reviewer #1 -- NCOMMS-25-43028 by Yimeng Li et al

> The manuscript by Li et al. presents the deformation of metal nanotips in high electrical fields, investigated in field emission transmission electron microscope (TEM). The work is methodologically flawless and delivers results that are obviously of current relevance.

Response:

We sincerely appreciate you taking the time to review our manuscript and provide professional comments. All the comments are greatly helpful for improving the quality of our work. We have carefully considered each comment and have made detailed revisions as best as we could. We hope the explanations and revisions can make the questions clear.

> 1. In the abstract, the authors somehow justify their submission by referring to a Nature paper without providing a citation (which, in my understanding, should not be done in an abstract). You probably mean reference 6?

Response:

Thank you for your comment. The *Nature* paper we referred to is Ref. [6] [Nikoo *et al.*, *Nature* **579**, 534–539 (2020)]. We have modified the related description in the revised manuscript:

Revised manuscript:

Lines 16-18:

Electric-field-induced effects severely impact the long-term stability and reliability of nanoelectronic devices with nanogaps, such as field emission nanodiodes, field-effect nanotransistors and ultrafast switches

> 2. The authors describe experiments on three different nanotips. I can't see from the paper why 3 nanotips need to be examined, surely one tip with a small radius and one with a large radius should be enough?

Response:

Thank you for your comment. In our experiments, we observed a clear size-dependent morphology evolution. When the apex radius of nanotip is greater than or equal to 9 nm, its morphology remains largely stable during field emission. For nanotips with apex radii below 9 nm, the morphology evolution depends strongly on the apex curvature, as even a few nanometers of difference in radius can lead to considerable changes in the surface-to-volume ratio and, consequently, the surface free energy. Specifically, nanotips with radii of 2 nm and 3 nm exhibit noticeable morphological changes primarily at the surface itself. At the same time, the 5 nm nanotip consists of sufficient number of atoms to exhibit the bulk effects along with the activities of the surface atoms. We see here that this large nanotip undergoes deformation through significant dislocation generation, annihilation, and regeneration. Therefore, we selected three representative nanotips to capture the critical transitions in their size-dependent deformation behavior and to provide a more comprehensive understanding of how curvature radius affects field emission-induced deformation at the nanoscale.

We have emphasized this size-dependent deformation in the revised manuscript:

Revised manuscript:

Lines 72-74:

These structural modifications show strong dependence on the size and crystallographic orientation of the nanotip.

Lines 379-384:

A distinct morphological evolution from spherical to polyhedral and back to near-spherical shape is observed in the 3 nm and 5 nm nanotips. The 9 nm tip, however, remains structurally unchanged. Furthermore, the 5 nm tip exhibits formation and annihilation of dislocations, which are negligible in the 3 nm tip. These results demonstrate a pronounced size-dependent effect in the structural deformation of the nanotips during the field emission process.

3. The work is based on the TEM experiments and therefore it would be good if the TEM used is briefly described (and a reference given) and there could also be a note on the microscope settings (acceleration voltage, angles, defocus, ...). The images are obviously TEM brightfield images and the stripes in the particles are probably lattice fringes (e.g. in Fig. 1)? For the TEM specimen holder, the company and the country should also be specified.

Response:

Thank you for your comment. We have provided the specific TEM testing procedure and parameters, and added the company and the country of TEM specimen holder in the revised manuscript:

Revised manuscript:

Lines 80-83:

The electrode deformation behaviors during field emission are tested using an in situ electrical measurement and micromorphology characterization system, which comprises a JEOL-2100F TEM (JEOL Ltd., Japan) and an in situ electrically biased TEM holder (ZEPTOOLS Technology Co., Ltd., China.)[33].

Lines 423-460:

The in situ electrical measurement and micromorphology characterization system consists of the JEOL-2100F TEM (JEOL Ltd., Japan) and an in situ electrically biased TEM holder (ZEPTOOLS Technology Co., Ltd., China.). This setup enables atomic-scale imaging with a point resolution of 0.23 nm and a line resolution of 0.10 nm, while allowing nanogap adjustment with an accuracy of 0.04 nm. The system can apply a direct current voltage of up to 150 V across nanogaps, with a current measurement resolution of 0.1 nA. The specific testing procedure and parameters are as follows: TEM operates at an accelerating voltage of 200 kV, and all measurements are performed at room temperature under a vacuum of ~10^{-5} Pa. Initially, the tungsten nanoelectrode (prepared by ex situ double-electrolyte electrochemical etching method) and the gold plate (prepared by pressing and cutting) are mounted on the TEM electrical holder, and then in situ Joule melting method is applied for the preparation of pure tungsten nanotips (see Fabrication of the pure tungsten nanotips in Methods section for details). After electrode preparation,

the fixed electrode (gold plate) is adjusted to the focal plane by tuning the Z-height. Subsequently, the movable electrode (tungsten nanotip) is brought into the same plane by finely controlling its displacement. To align the viewing direction parallel to a crystallographic zone axis, the TEM holder is carefully tilted using the goniometer stage, typically within a range of 5-10°. Kikuchi lines are used as references to guide alignment along an appropriate zone axis, while the heights of both electrodes are adjusted to maintain focus. The SAED patterns are then acquired at the apex under a magnification of 500-800× to confirm the crystal orientation of the tungsten nanotip. The Supplementary Fig. 3, Fig. 15a and Fig. 16a show the post-processed SAED patterns, in which image rotation (to match the HRTEM viewing direction), contrast enhancement, and spot labeling were applied to improve clarity and facilitate crystallographic analysis.

Subsequently, the magnification is gradually increased to 1.0-1.5 M×, and the electrode gap is adjusted to approximately 15 nm. The sample is then removed, and the electron beam is spread to achieve a low current density of ~4 pA/cm^2 (~4×10^{-14} pA/nm^2), measured on a 160 mm-diameter screen. When the sample is moved back into the beam, this current density can be considered as the beam current density (dose rate) at the specimen. The corresponding total beam current is approximately 144 μA, provided here for reference only, as beam spreading and aperture limitations decouple this value from the actual dose on the nanotip. The camera (Gatan 833 Orius SC200D) is then inserted to capture high-resolution TEM (HRTEM) images of the nanotip in real time. Live Fast Fourier transform (FFT) analysis is performed using DigitalMicrograph software to correct objective lens astigmatism by adjusting the deflector until the FFT halo appears circular. Final focusing is achieved by adjusting the focus knobs until the diffraction rings expand to infinity, under a slight defocus condition (typically in the range of -50 nm to -100 nm) to enhance lattice contrast. This configuration enables high-resolution, real-time observation of nanotip deformation behavior under applied electric fields and during field emission. It should be noted that no spherical aberration correction is applied (Cs = 0.0 mm).

In addition, the HRTEM images shown (e.g., Fig. 1) are indeed TEM bright-field images. The stripe-like features observed within nanotips are identified as lattice fringes, which reflect the periodic arrangement of atomic planes in the crystalline structure. The uniformity and continuity of these fringes across the nanotip further support their crystallographic origin. It is also worth noting that the slight extension of the fringes beyond the nanotip boundary may result from the delocalization effect, which commonly occurs in bright-field TEM imaging, especially under underfocused conditions. In our in situ experiments, the nanotip gradually developed a slight downward tilt during prolonged field emission treatment—likely due to its own weight—which may have increased the defocus and thereby enhanced this effect. Nevertheless, such an effect can be mitigated during the observation periods by carefully adjusting the tip height. We have explicitly emphasized this point in the revised manuscript:

Revised manuscript:

Lines 113-121:

Notably, some blurry boundaries in these TEM images are attributed to the delocalization effect[37], which commonly occurs in bright-field TEM imaging, especially under

underfocused conditions. In our in situ experiments, the nanotip gradually developed a slight downward tilt by its own weight during prolonged field-emission treatment, which caused additional defocus, thereby enhancing blurriness of the boundaries. This can be mitigated during the observation periods by careful adjustment of the tip height. Although electron-beam delocalization may cause a certain degree of image blurring, the comparison of the nanotip at different time intervals clearly reveals distinct morphological changes that may result from several physical processes triggered by combination of the applied field and the field emission process.

4. The labelling in most of the images is difficult to read as it is too small. This also applies to the mu dashes, which definitely needs to be corrected.

Response:

Thank you for your valuable comment. We have carefully revised all figures (Fig. 1 to Fig. 4):

Revised manuscript:

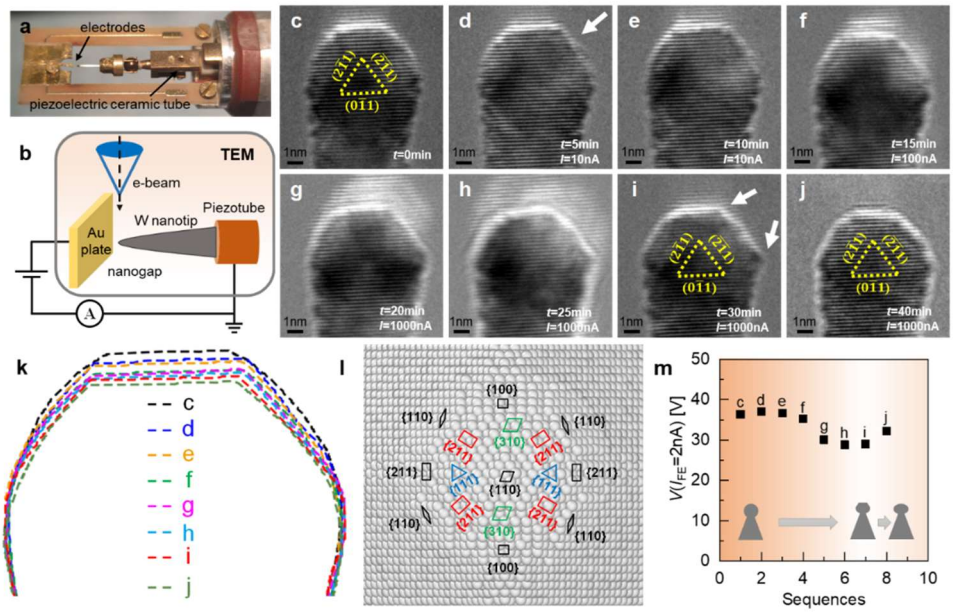

Fig. 1 a The in situ electrically biased TEM holder. **b** The schematic diagram of the in situ electrical measurement and micromorphology characterization system. **c-j** TEM images showing the progressive deformation behaviors of a <110>-oriented tungsten nanotip with an apex radius of 3 nm during field emission. The corresponding field emission current (I_{FE}) and the cumulative treatment time (t) are indicated in the lower right corner of each image. **k** The surface profiles of tungsten nanotips. **l** The top view of an atomistic model illustrating a <110>-oriented tungsten nanotip with an apex radius of 3 nm. **m** The applied voltages required to achieve a field emission current of 2 nA (d = 15 nm) is plotted in relation to the morphology changes of this tungsten nanotip.

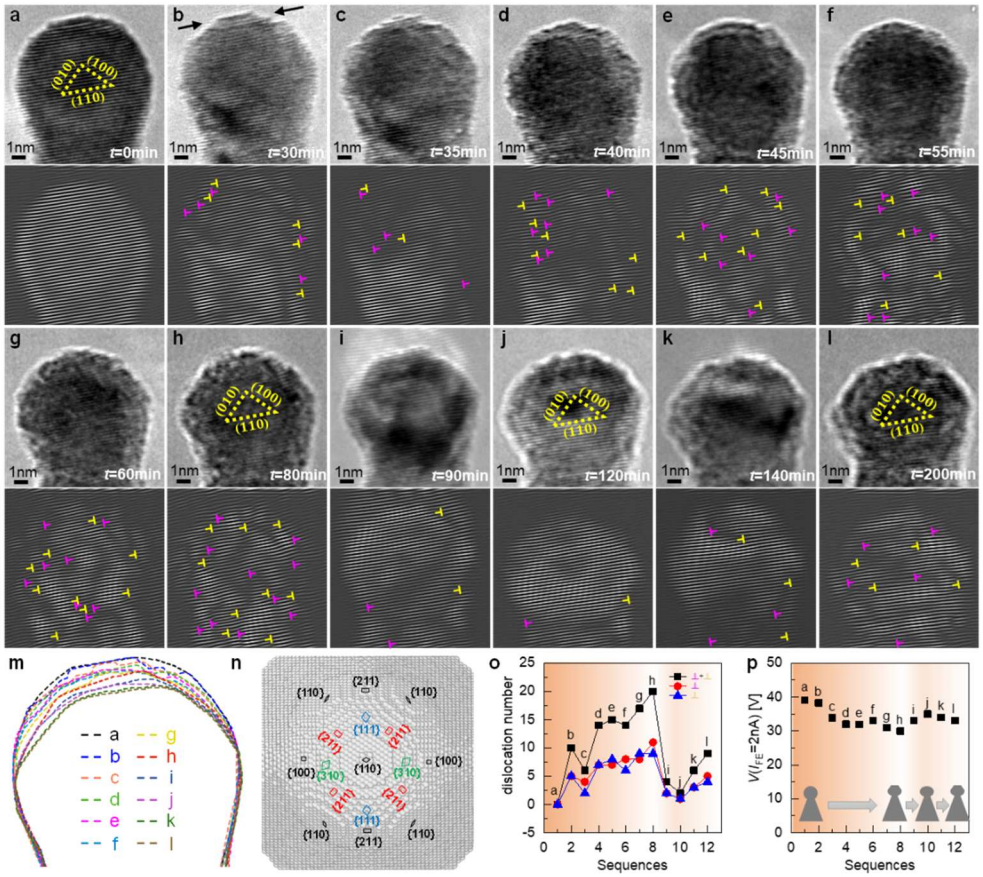

Fig. 2 a-l TEM images showing the progressive deformation behaviors of a <110>-oriented tungsten nanotip with an apex radius of 5 nm after each field emission treatment (I_{FE} = 1000 nA) period. Below each TEM image, the corresponding Fourier-filtered images depict the evolution of dislocations, with the edge dislocations of different polarities marked by magenta and yellow '⊥' symbols, respectively. The cumulative treatment time (t) are indicated in the lower right corner of each TEM image. **m** The collection of all morphological profiles. **n** The top view of an atomistic model illustrating a <110>-oriented tungsten nanotip with an apex radius of 5 nm. **o** The total numbers of dislocations, along with the numbers of dislocations of different polarities for each nanotip morphology. **p** The applied voltages required to achieve a field emission current of 2 nA (d = 15 nm) is plotted in relation to the morphology changes of this tungsten nanotip.

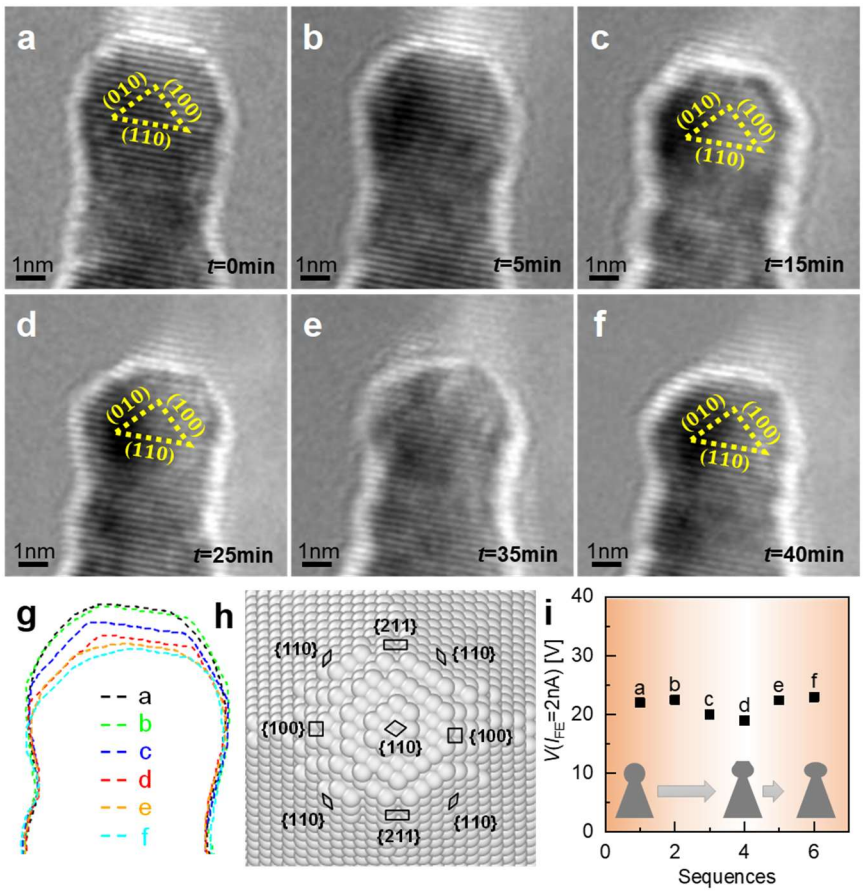

Fig. 3 a-f TEM images showing the progressive deformation behaviors of a <110>-oriented tungsten nanotip with an apex radius of 2 nm during the reverse polarity treatment. The cumulative treatment time (*t*) are indicated in the lower right corner of each image. **g** The collection of all morphological profiles. **h** The top view of an atomistic model illustrating a <110>-oriented tungsten nanotip with an apex radius of 2 nm. **i** The applied voltages required to achieve a field emission current of 2 nA (*d* = 15 nm) is plotted in relation to the morphology changes of this tungsten nanotip.

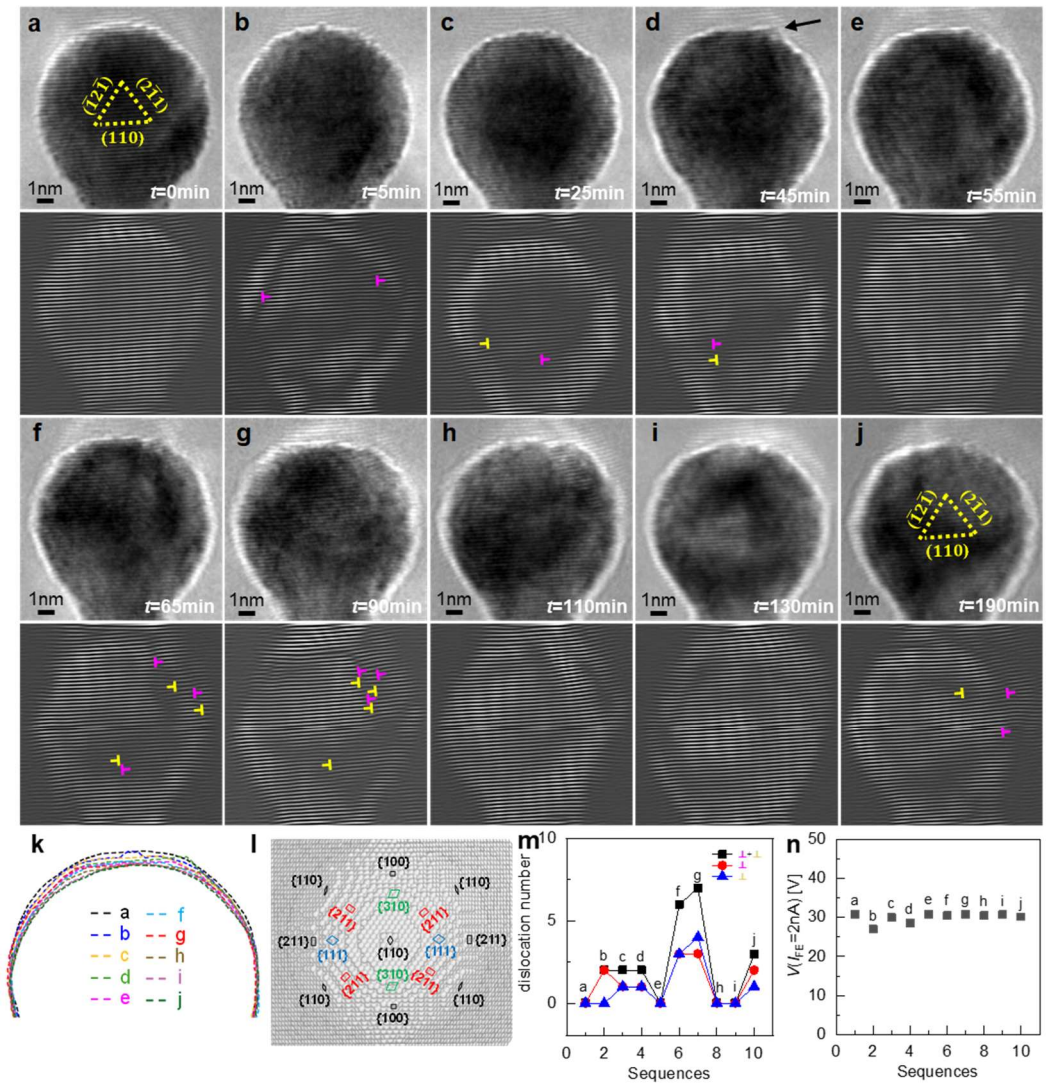

Fig. 4 a-j TEM images showing the progressive deformation behaviors of a <110>-oriented tungsten nanotip with an apex radius of 5 nm during reverse polarity treatment. The cumulative treatment time (*t*) are indicated in the lower right corner of each image. Below each TEM image, the corresponding Fourier-filtered images depict the evolution of dislocations, with the edge dislocations of different polarities marked by magenta and yellow '⊥' symbols, respectively. **k** The collection of all morphological profiles. **l** The top view of an atomistic model illustrating a <110>-oriented tungsten nanotip with an apex radius of 5 nm. **m** The total numbers of dislocations, along with the numbers of dislocations of different polarities for each nanotip morphology. **n** The applied voltages required to achieve a field emission current of 2 nA (*d* = 15 nm) is plotted in relation to the morphology changes of this tungsten nanotip.

5. The authors use the term SAED images (selected area electron diffraction) for some images (Fig. 3, 11 and 12 in the supplement), but strictly speaking these are not classical SAED images but Fourier transformations (diffractograms) of the corresponding TEM images.

Response:

Thank you for your valuable comment. We would like to clarify that Supplementary Fig. 3, Fig. 15a

(original Fig. 11a), and Fig. 16a (original Fig. 12a) present post-processed selected area electron diffraction (SAED) patterns (obtained using a selected area aperture in TEM). Since the tip orientation during SAED acquisition (under a magnification of 500-800×) was different from that used for high-resolution TEM (HRTEM) imaging (under a magnification of 1.0-1.5 M×), the SAED images were rotated during post-processing to align them with the corresponding HRTEM images for clearer structural analysis. Additionally, contrast enhancement and spot labeling were applied to improve the visibility of diffraction spots. Figure R1 presents the tip orientation at low magnification along with the raw SAED pattern, while Figure R2 shows the tip orientation during HRTEM imaging together with the post-processed SAED pattern.

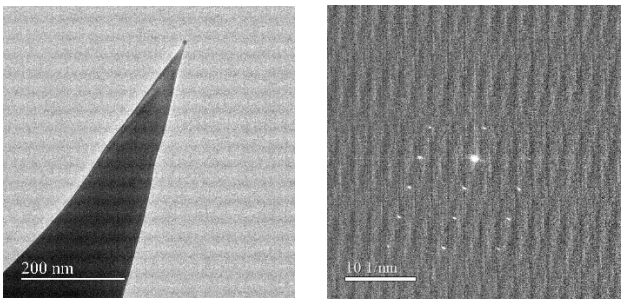

Figure R1. Tip orientation at low magnification along with the raw SAED pattern for 5 nm tungsten nanotip

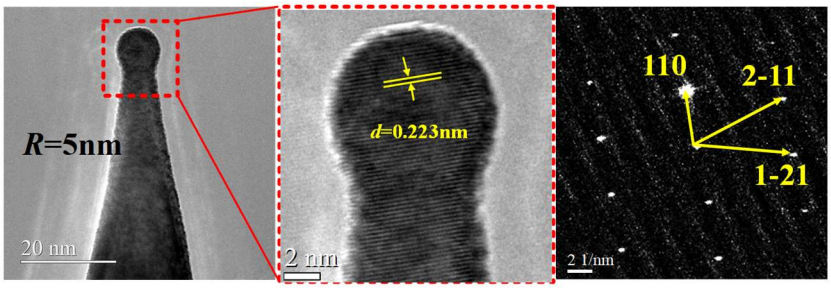

Figure R2. Tip orientation during HRTEM imaging along with the post-processed SAED pattern for 5 nm tungsten nanotip

We have revised the figure captions and relevant descriptions in the revised manuscript and supplementary information to clearly indicate that these are measured SAED patterns with post-processing applied.

Revised manuscript:

Lines 415-419:

The TEM images and the post-processed selected area electron diffraction (SAED) patterns of the initial tungsten nanotips with different radii (R=3 nm, 5 nm and 9 nm) depicted in Supplementary Fig. 3a-c reveal a surface devoid of contaminants, a round and smooth apex, a neatly arranged lattice with few internal defects and a <110> crystallographic direction parallel to the emitter axis.

Lines 435-445:

After electrode preparation, the fixed electrode (gold plate) is adjusted to the focal plane by tuning the Z-height. Subsequently, the movable electrode (tungsten nanotip) is brought

into the same plane by finely controlling its displacement. To align the viewing direction parallel to a crystallographic zone axis, the TEM holder is carefully tilted using the goniometer stage, typically within a range of 5-10°. Kikuchi lines are used as references to guide alignment along an appropriate zone axis, while the heights of both electrodes are adjusted to maintain focus. The SAED patterns are then acquired at the apex under a magnification of 500-800× to confirm the crystal orientation of the tungsten nanotip. The Supplementary Fig. 3, Fig. 15a and Fig. 16a show the post-processed SAED patterns, in which image rotation (to match the HRTEM viewing direction), contrast enhancement, and spot labeling were applied to improve clarity and facilitate crystallographic analysis.

Supplementary Information:

Lines 21-23:

Supplementary Fig. 3| The TEM images of the initial tungsten nanotips with different apex radii (R = 3 nm, 5 nm and 9 nm) and the corresponding post-processed selected area electron diffraction (SAED) results. (a) R = 3 nm. (b) R = 5 nm. (c) R = 9 nm.

Lines107-108:

The corresponding TEM images and post-processed SAED results are shown in Supplementary Fig. 15a and Supplementary Fig. 16a

Line 120:

The TEM images of this tungsten nanotip and the corresponding post-processed SAED result

Line 126:

The TEM images of this tungsten nanotip and the corresponding post-processed SAED result

6. Try to improve the conclusions, a clearer structure would be fine.

Response:

Thank you for your valuable suggestion. We have carefully revised the conclusion section to improve its clarity, logical structure, and overall readability. The revised conclusion is as follows:

Revised manuscript:

Lines 377-392:

In conclusion, the deformation behavior during field emission process of typical metal nanostructures, i.e., tungsten nanotips with different radii (R = 3 nm, 5 nm and 9 nm) is studied *in situ* at room temperature using an electrical testing platform integrated with TEM. A distinct morphological evolution from spherical to polyhedral and back to near-spherical shape is observed in the 3 nm and 5 nm nanotips. The 9 nm tip, however, remains structurally unchanged. Furthermore, the 5 nm tip exhibits formation and annihilation of dislocations, which are negligible in the 3 nm tip. These results demonstrate a pronounced size-dependent effect in the structural deformation of the nanotips during the field emission process. At the same time, the less pronounced structural changes in the 5 nm nanotip during the reverse polarity experiments confirm that the field emission is able to

drive the structural transformations within metal nanotips via electron wind forces and the associated field-assisted evaporation. We also find that even in the absence of field emission currents, the significant morphological changes in small nanotips ($R < 3$ nm) are caused by substantial direct field evaporation at the electric fields (10-13 V/nm) lower than previously reported thresholds (40-60 V/nm). These findings provide direct microscopic evidence for electric-field-induced structural transformations in metallic nanostructures and offer valuable insights into the reliability and failure mechanisms of nanoelectronic devices.

Report of Reviewer #2 -- NCOMMS-25-43028 by Yimeng Li et al

The authors present an in situ TEM study investigating the mechanisms behind electric-field-induced structural and morphological changes of tungsten nanotips during field emission. The use of a specialized and quite uncommon TEM holder enables direct visualization of these changes, which is the major strength of the study. The experimental approach is intriguing, and the opportunity to observe such electric-field-driven phenomena in real-time offers significant value to the field. However, while the results are interesting, I find that several aspects of the interpretation, presentation, and methodological clarity require further attention before the manuscript can be considered for publication in such a high impact journal.

Response:

We greatly appreciate the time and effort you have dedicated to reviewing our manuscript and providing valuable comments. All the comments have been greatly helpful in enhancing the quality of our work. We have carefully considered each point and made revisions as best as we could. We hope the explanations and revisions clarify the issues raised.

1. The manuscript states already in the abstract (but also later in the manuscript that the threshold for field-induced atom evaporation is reduced by a factor of five compared to theoretical predictions. However, it remains unclear how this factor is determined, and which reference values are used for comparison. Two of the cited studies (Golubov and Tamaki & Kuroda) also report experimental results rather than purely theoretical values, contrary to the claim in the manuscript. A clear and quantitative justification of the comparison, including the experimental conditions under which the cited value was obtained, is needed for this claim to be substantiated.

Response:

We thank the reviewer for pointing out this ambiguity. To improve on the clarity of our claim, we have revised the manuscript by replacing the terms “theoretical prediction” or “theoretical values” with the more accurate “previously reported values”. Next, we have provided a detailed comparison with both a theoretical study (Ashton et al., *Phys. Rev. Lett.* 124, 176801 (2020)) and an experimental study (Golubev, *Tech. Phys. Lett.* 40, 1092–1094 (2014)), explicitly presenting their reported threshold values and contrasting them with our experimental observations. The revised part in the manuscript is as follows:

Revised manuscript:

Lines 22-24:

We find that electron wind effects and nanoscale effects dramatically reduce the atom evaporation threshold to 10-13 V/nm, which is approximately one-fourth to one-fifth of the previously reported values of 40-60 V/nm.

Lines 262-284:

As can be seen in the reverse polarity experiments, we observe field evaporation without Joule heating or electron wind effects, particularly the evaporation of edge atoms. The

maximum local electric field of 2 nm nanotip is highest among different nanotips and reaches about 13.0 V/nm for spherical shape (Supplementary Fig. 18), with a slight increase (13.3 V/nm) for polyhedral geometry. Although the simulated model is idealized, the differences between simulated models and realistic structures are not significant[39]. It is surprising that atom evaporation in our experiments occurs at the electric field values of 10-13 V/nm (see Supplementary Note 1 and Supplementary Fig. 18) because they are significantly lower than the previously reported thresholds of 40-60 V/nm[40,41]. Specifically, in the theoretical study by Ashton et al.[41], the field-induced bond breaking at kink sites on high-index tungsten surfaces was studied using density functional theory (DFT) with the generalized dipole correction (GDC) method. They identified a two-stage field evaporation mechanism: the atom first rolls over from the constrained step edge position to a neighboring hollow site on the adjacent terrace surface, from where the atom detaches. At low electric fields, the second step has a high energy barrier. As the electric field increases, this barrier decreases until it is lower than the roll-over barrier at ~42 V/nm. Above this threshold, the evaporation proceeds as effectively a single-stage process. This analysis indicates that even for kink sites, the theoretical evaporation threshold exceeds 42 V/nm. Experimentally, Golubev et al.[40] developed a method to determine the field evaporation threshold based on current-voltage measurements in a field-electron microscope. Using this approach, they reported a threshold value of approximately 57 V/nm for tungsten point emitters with tip radii of about 1 μm. In our experiments, this lowered threshold of 10-13 V/nm can be attributed to the enhanced local field and the lower number of neighboring atoms at edge sites[22,24,42], especially at the edges of the atomic terraces and on the top plane, which are strongly influenced by the apex radius of the nanotip.

39. Li, Y. M., Xia, L. H., Li, N., Tang, S. L., Ge, Y. S., Wang, J. Y., Xiao, B., Cheng, Y. H., Ang, L. K., Meng, G. D. Uncovering a widely applicable empirical formula for field emission characteristics of metallic nanotips in nanogaps. *Nat Commun* **16**, 5583 (2025).
40. Golubev, O. L. Experimental determination of evaporating electric field strengths for nanodimensional field ion emitters. *Tech Phys Lett* **40**, 1092-1094 (2014).
41. Ashton, M., Mishra, A., Neugebauer, J., Freysoldt, C. Description of Bond Breaking in Large Electric Fields. *Phys Rev Lett* **124**, 176801 (2020).

Supplementary Information:

Lines 38-56:

Supplementary Note 1: The simulated electric field distribution for atomistic models

Based on the established model (a typical example is shown in Supplementary Fig. 7), the atomically mapped field distributions of spherical and polyhedral nanotips with apex radii of 3 nm, 5 nm, and 9 nm are shown in Supplementary Figs. 8-10. It can be seen that the electric field is stronger at the edge atoms, and the polyhedral nanotips exhibit only a slight increase in field strength compared with the spherical ones.

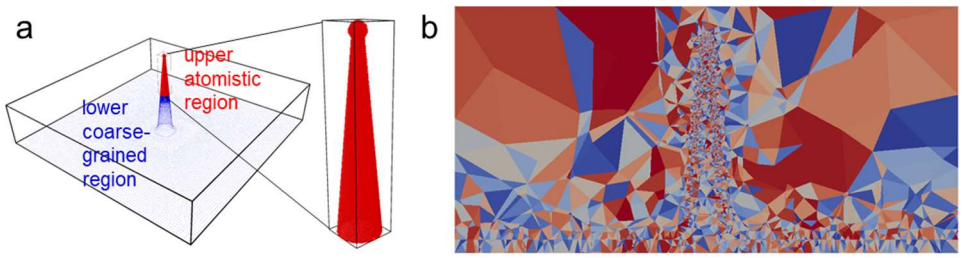

Supplementary Fig. 7| The typical nanotip model in FEcMD simulation. (a) The nanotip model. (b) The finite element mesh.

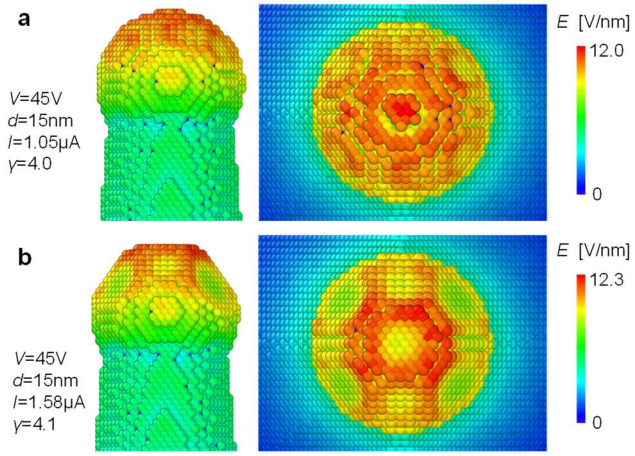

Supplementary Fig. 8| The electric field distribution for the atomistic spherical nanotip and the polyhedral nanotip with a 3 nm apex radius. (a) The spherical nanotip. (b) The polyhedral nanotip.

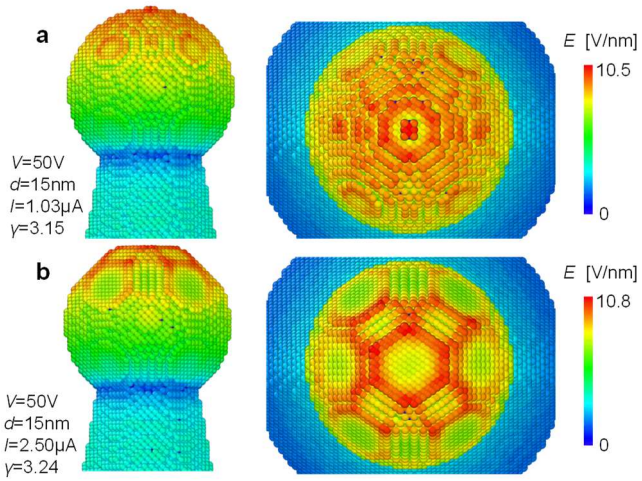

Supplementary Fig. 9| The electric field distribution for the atomistic spherical nanotip and the polyhedral nanotip with a 5 nm apex radius. (a) The spherical nanotip. (b) The polyhedral nanotip.

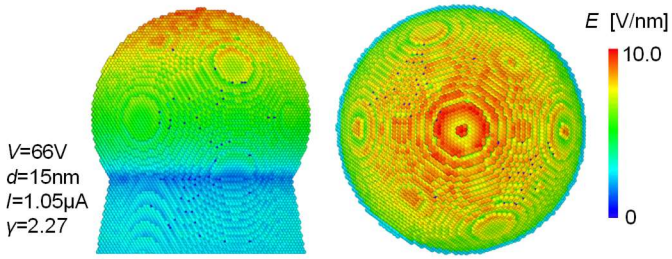

Supplementary Fig. 10| The electric field distribution for the atomistic spherical nanotip with a 9 nm apex radius.

Lines 136-138:

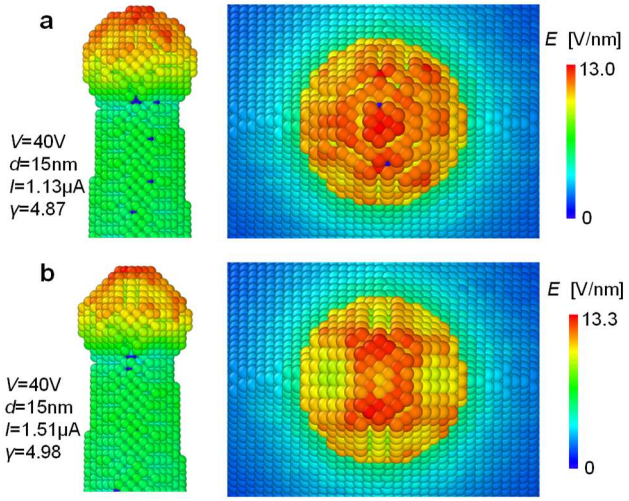

Supplementary Fig. 18| The electric field distribution for the atomistic spherical nanotip and the polyhedral nanotip with a 2 nm apex radius. (a) The spherical nanotip. (b) The polyhedral nanotip.

2. While the authors conclude that beam-induced heating is probably negligible under the conditions used (as supported by prior literature, e.g., Egerton, 10.1016/j.micron.2004.02.003), they do not adequately address other beam effects, such as elastic displacement interactions with tungsten nuclei (aka knock-on displacements, also see Egerton). The manuscript claims the morphology remains " essentially unchanged", but does not clarify whether this applies to more subtle atomic-scale features, such as the distribution of dislocations, adatom motion, or local diffusion processes at edges or corners. Prior studies (e.g., 10.1063/1.5093472; 10.1017/S1431927612014274) have shown that beam irradiation can enhance diffusion and defect mobility, especially at metallic surfaces and low-coordination sites. A deeper discussion of these possible effects is needed.

Response:

Thank you for your professional comment. In our experiments, the TEM was operated at an accelerating voltage of 200 kV (incident electron energy of 200 keV). The beam current density

(dose rate) at the specimen was obtained approximately from the read-out of current density on the viewing screen, without specimen. In our experiments, the electron beam was spread to achieve a low beam current density (dose rate) of ~4 pA/cm^2 (~4×10^{-14} pA/nm^2), measured on a 160 mm-diameter screen. Under electron-beam irradiation, various effects may occur in the electrodes, such as beam-induced heating, elastic displacement interactions, electron-beam sputtering [Egerton et al., Micron 35, 399-409, 2004], which need to be carefully considered and evaluated in the context of our experiments.

（i）For electron-beam sputtering of tungsten, the threshold incident electron energy is about 500 keV (> 200 keV), and thus it can be neglected under our experimental conditions.

（ii）For beam-induced heating, the temperature rise caused by electron beam at a dose rate of ~4 pA/cm^2 is minimal (<1 K) [Figure 4.11 in Williams et al., The transmission electron microscope. Springer (1996); Sun et al., Nat. Mater. 13, 1007-1012, 2014; Egerton et al., Micron 35, 399-409, 2004].

（iii）For elastic displacement interactions, the surface diffusion energy E_{sd} of tungsten is about 0.8 eV [Yang et al., J. Phys.: Condens. Matter 23, 395004, 2011], which is typically lower than the adsorption energy E_{ad} by a factor of three or more [Egerton, Microsc. Microanal. 19, 479-486, 2013]. This E_{sd} value corresponds to a threshold incident electron energy of approximately 220 keV. In our experiments, the electron energy is 200 keV, which is close to this threshold, suggesting that beam-induced surface diffusion may occur. To further assess this possibility, the beam-induced surface-displacement rate (see Eq. 10 in [Egerton, Microsc. Microanal. 19, 479-486, 2013]), which is proportional to the beam current density, was estimated. Based on E_{sd} = 0.8 eV, J = 4 pA/cm^2, and the atomic number of tungsten Z = 74 (see Fig. 4 in [Egerton, Microsc. Microanal. 19, 479-486, 2013]), the displacement rate would be on the order of 10^{-13} s^{-1}. In our experiments, although the nanotip surface contains atomic steps where atoms may preferentially diffuse along step edges due to lower E_{sd} (~0.58 eV) [Yang et al., J. Phys.: Condens. Matter 23, 395004, 2011], a one-order-of-magnitude difference in the displacement rate (see Fig. 4 in [Egerton, Microsc. Microanal. 19, 479-486, 2013]) is insufficient to produce significant beam-induced knock-on displacement to contribute surface atom diffusion, and is likewise unlikely to initiate or drive the motion of dislocations. Therefore, although the beam energy is close to the threshold incident electron energy for surface diffusion, the very low beam current density (far below the field emission densities ~10^6 A/cm^2) ensures that knock-on displacement can be neglected.

We have added the discussion about the electron beam effects in the revised manuscript and Supplementary Information:

Revised manuscript:

Lines 367-375:

In addition, the electron beam can induce electron-beam sputtering, beam-induced heating, elastic displacement interactions, and hydrocarbon contamination, among other effects[57]. In our experiments, the low beam current density (~4 pA/cm^2) allows electron-beam sputtering, beam-induced heating, and elastic displacement interactions to be neglected (see Supplementary Note 6). The high vacuum level (~10^{-5} Pa), low beam current density (~4 pA/cm^2) and relatively high field emission current density (which helps to clean the tip surface) render beam-induced hydrocarbon contamination negligible[58,59]. Therefore, the effects of the imaging electron beam are insignificant for the morphology evolution

observed in our experiments.

57. Egerton, R. F., Li, P., Malac, M. Radiation damage in the TEM and SEM. *Micron* **35**, 399-409 (2004).
58. de Parga, A. L. V., Hernan, O. S., Miranda, R., Yeyati, A. L., Mingo, N., Martin-Rodero, A., Flores, F. Electron resonances in sharp tips and their role in tunneling spectroscopy. *Phys Rev Lett* **80**, 357-360 (1998).
59. Feenstra, R. M., Stroscio, J. A., Fein, A. P. Tunneling Spectroscopy of the Si(111)2x1 Surface. *Surf Sci* **181**, 295-306 (1987).

Supplementary Information:

Lines 171-210:

Supplementary Note 6: The electron beam effects of TEM on the deformation behavior of nanotip

Under TEM, the electron beam may induce various effects in the electrodes, such as electron-beam sputtering, beam-induced heating, elastic displacement interactions, and beam-induced hydrocarbon contamination[3], which also need to be carefully considered and evaluated. In our experiments, the TEM was operated at an accelerating voltage of 200 kV (incident electron energy of 200 keV). During real-time observation of morphological evolution, the electron beam was spread to achieve a low current density (dose rate) of ~4 pA/cm^2, measured on a 160 mm-diameter screen. (i) For electron-beam sputtering of tungsten, the threshold incident electron energy is about 500 keV, and thus it can be neglected under our experimental conditions (~200 keV). (ii) For beam-induced heating, the temperature rise caused by electron beam at a dose rate of ~4 pA/cm^2 is minimal (<1 K)[3-5]. (iii) For elastic displacement interactions, the surface diffusion energy E_{sd} of tungsten is about 0.8 eV[6], which is typically lower than the adsorption energy E_{ad} by a factor of three or more[7]. This E_{sd} value corresponds to a threshold incident electron energy of approximately 220 keV. In our experiments, the electron energy is 200 keV, which is close to this threshold, suggesting that beam-induced surface diffusion may occur. To further assess the contribution of beam-induced effects, we estimated the beam-induced surface-displacement rate (see Eq. 10 in Ref. 7), which is proportional to the beam current density. Given E_{sd} = 0.8 eV, J = 4 pA/cm^2, and the atomic number of tungsten Z = 74 (see Fig. 4 in Ref. 7), we obtain the displacement rate to be on the order of 10^{-13} s^{-1} [7]. In our experiments, although the nanotip surface contains atomic steps where atoms may preferentially diffuse along step edges due to lower E_{sd} (~0.58 eV)[6], a one-order-of-magnitude difference (see Fig. 4 in Ref. 7) in the displacement rate is insufficient to produce significant beam-induced knock-on displacement to contribute surface atom diffusion[7]. This low rate is also insufficient to generate the point-defect density needed to nucleate dislocations or to drive the migration of pre-existing ones. This is confirmed by the clear difference in the TEM images obtained for the same nanotip in both polarities of the applied field. As we can see, although the beam energy is close to the threshold incident electron energy for surface diffusion, the very low beam current density (far below the field emission densities ~10^6 A/cm^2) ensures that knock-on displacement can be neglected. (iv) It is also known that the beam-induced hydrocarbon contamination may

occur during the TEM imaging[3], however, no obvious amorphous carbon layer was observed during several hours of morphological evolution (~10^{-5} Pa vacuum level in TEM) (Fig. 2 and Fig. 4), in contrast to our earlier SEM observations at high magnification (Supplementary Fig. 21), where pronounced amorphous carbon deposition occurred within seconds. Moreover, during field emission, the field-emission characteristics remained relatively stable, without noticeable fluctuations (see Supplementary Fig. 2 and Supplementary Fig. 5), unlike our previous observation of fluctuating field-emission behavior in a carbon-coated tungsten nanotip[8]. Since the tungsten tip acts as an electron source during field emission, the high current density can even help to clean the tip surface[9,10]. Therefore, we can state with the confidence that the effects of the imaging electron beam are insignificant for the morphology evolution observed in our experiments.

3. Egerton, R. F., Li, P., Malac, M. Radiation damage in the TEM and SEM. *Micron* 35, 399-409 (2004).
4. Sun, J., He, L. B., Lo, Y. C., Xu, T., Bi, H. C., Sun, L. T., Zhang, Z., Mao, S. X., Li, J. Liquid-like pseudoelasticity of sub-10-nm crystalline silver particles. *Nat Mater* 13, 1007-1012 (2014).
5. Williams, D. B., Carter, C. B. The transmission electron microscope. In: *Transmission electron microscopy: a textbook for materials science*). Springer (1996).
6. Yang, J. Y., Hu, W. Y., Tang, J. F. Surface self-diffusion behavior of individual tungsten adatoms on rhombohedral clusters. *J Phys-Condens Mat* 23, 395004 (2011).
7. Egerton, R. F. Beam-Induced Motion of Adatoms in the Transmission Electron Microscope. *Microsc Microanal* 19, 479-486 (2013).
8. Meng, G., Li, Y., Koitermaa, R. A., Zadin, V., Cheng, Y., Kyritsakis, A. In Situ Observation of Field-Induced Nanoprotrusion Growth on a Carbon-Coated Tungsten Nanotip. *Phys Rev Lett* 132, 176201 (2024).
9. de Parga, A. L. V., Hernan, O. S., Miranda, R., Yeyati, A. L., Mingo, N., Martin-Rodero, A., Flores, F. Electron resonances in sharp tips and their role in tunneling spectroscopy. *Phys Rev Lett* 80, 357-360 (1998).
10. Feenstra, R. M., Stroscio, J. A., Fein, A. P. Tunneling Spectroscopy of the Si(111)2x1 Surface. *Surf Sci* 181, 295-306 (1987).

In addition, the statement that the morphology of the 9 nm nanotip remains “essentially unchanged” refers to the overall geometric profile of the tip, which shows no observable variation after 4 hours of field emission treatment (I_{FE} = 1000 nA, current density 3.90 ×10^5 A cm^{-2}). According to the previous analysis of the electron beam effects, the beam-induced atomic knock-on displacements on the surface and within the bulk are negligible. We acknowledge that a very limited degree of atomic activity—particularly localized diffusion of surface atoms at edges and corners—may still occur due to field emission. Considering the large number of atoms in a nanotip with a curvature radius of 9 nm, the impact of such atomic motions on the overall morphology is minimal. Furthermore, the number of atomic layers shows no significant reduction. These processes are therefore expected to be confined to the near-surface region and are insufficient to induce any measurable morphological change in our experiment. The corresponding clarification has been added in the revised manuscript:

Revised manuscript:

Lines 183-187:

However, it can be seen that the morphology of this tungsten nanotip exhibits no significant change, where the number of atomic layers shows no significant reduction and the tip is influenced only by a very limited degree of atomic activity, primarily involving localized surface atoms. The field emission capability remains largely unchanged.

3. Key experimental parameters are missing, which limits reproducibility. Paramters like electron energy, beam current, and dose rate should be specified. Additional imaging parameters, such as illumination/imaging settings and camera model, should also be included, together with details on the processing steps applied to the images (eg. FFT filtering). It would be useful to comment on whether electric field conditions during imaging or other experimental issues may have affected image contrast or resolution (referring to the delocalization effect mentioned in line 110 which is visible in the images).

Response:

Thank you for your valuable comment. We have included the specific testing procedure and parameters in the revised manuscript:

Revised manuscript:

Lines 423-460:

The in situ electrical measurement and micromorphology characterization system consists of the JEOL-2100F TEM (JEOL Ltd., Japan) and an in situ electrically biased TEM holder (ZEPTOOLS Technology Co., Ltd., China.). This setup enables atomic-scale imaging with a point resolution of 0.23 nm and a line resolution of 0.10 nm, while allowing nanogap adjustment with an accuracy of 0.04 nm. The system can apply a direct current voltage of up to 150 V across nanogaps, with a current measurement resolution of 0.1 nA. The specific testing procedure and parameters are as follows: TEM operates at an accelerating voltage of 200 kV, and all measurements are performed at room temperature under a vacuum of ~10^{-5} Pa. Initially, the tungsten nanoelectrode (prepared by ex situ double-electrolyte electrochemical etching method) and the gold plate (prepared by pressing and cutting) are mounted on the TEM electrical holder, and then in situ Joule melting method is applied for the preparation of pure tungsten nanotips (see Fabrication of the pure tungsten nanotips in Methods section for details). After electrode preparation, the fixed electrode (gold plate) is adjusted to the focal plane by tuning the Z-height. Subsequently, the movable electrode (tungsten nanotip) is brought into the same plane by finely controlling its displacement. To align the viewing direction parallel to a crystallographic zone axis, the TEM holder is carefully tilted using the goniometer stage, typically within a range of 5-10°. Kikuchi lines are used as references to guide alignment along an appropriate zone axis, while the heights of both electrodes are adjusted to maintain focus. The SAED patterns are then acquired at the apex under a magnification of 500-800× to confirm the crystal orientation of the tungsten nanotip. The Supplementary Fig. 3, Fig. 15a and Fig. 16a show the post-processed SAED patterns, in which image rotation (to match the HRTEM viewing direction), contrast enhancement, and spot labeling were applied to improve clarity and facilitate crystallographic analysis.

Subsequently, the magnification is gradually increased to 1.0-1.5 M×, and the electrode

gap is adjusted to approximately 15 nm. The sample is then removed, and the electron beam is spread to achieve a low current density of ~4 pA/cm^2 (~4×10^{-14} pA/nm^2), measured on a 160 mm-diameter screen. When the sample is moved back into the beam, this current density can be considered as the beam current density (dose rate) at the specimen. The corresponding total beam current is approximately 144 μA, provided here for reference only, as beam spreading and aperture limitations decouple this value from the actual dose on the nanotip. The camera (Gatan 833 Orius SC200D) is then inserted to capture high-resolution TEM (HRTEM) images of the nanotip in real time. Live Fast Fourier transform (FFT) analysis is performed using DigitalMicrograph software to correct objective lens astigmatism by adjusting the deflector until the FFT halo appears circular. Final focusing is achieved by adjusting the focus knobs until the diffraction rings expand to infinity, under a slight defocus condition (typically in the range of -50 nm to -100 nm) to enhance lattice contrast. This configuration enables high-resolution, real-time observation of nanotip deformation behavior under applied electric fields and during field emission. It should be noted that no spherical aberration correction is applied (Cs = 0.0 mm).

We have also provided the imaging parameters in the revised manuscript:

Lines 482-455:

After the treatment period, the observation period starts, during which high-resolution TEM imaging (Gatan 833 Orius SC200D, binning 1×1, exposure time 0.5 s) is performed to characterize the nanotip morphology, and the field emission characteristics at 15 nm nanogap are tested.

We have also included a detailed description of the image processing procedures:

Lines 488-494:

Fourier-filtered image processing is performed using DigitalMicrograph (Gatan) software. First, the apex region of the nanotip is selected and subjected to FFT. In the resulting FFT pattern, a pair of symmetric diffraction spots corresponding to the desired lattice spacing is selected using the *Add Spot Mask* tool. The mask is applied via the *Apply Mask and Apply Filter* option, with edge smoothing set to 5 pixels and the masked area retained. An inverse FFT (IFFT) is then performed to generate a filtered image that enhances lattice contrast and reveals dislocation features more clearly.

We have also discussed the effect of the electric field on the real-time TEM images:

Lines 474-482:

Although field emission at 10-13 V/nm slightly reduces imaging resolution, the effect is relatively minor (see Supplementary Video 1). This can be attributed to the slight defocus condition (-50 to -100 nm) in our experiments[60], and the negligible charge accumulation due to the absence of substantial surface contamination (e.g., carbon or oxide, unlike the nanotip in Supplementary Fig. 21)[60]. As a result, real-time monitoring remains effective for tracking the evolution and adjusting parameters. Due to nanosize effects and slight differences in current density, tips with different curvature radii evolve at different rates, so the parameters are therefore tailored to capture the entire deformation process, which

is essential for comparing the deformation behaviors of different tips.

60. Zhu, F., Li, W. P., Yeung, M. C., Zhang, Y. X., Du, C. C., Lin, B., Wang, Q., Guo, X. F., Hsueh, Y. C., Chen, F. R., Zhong, X. Y. Quantitative Determination of High-Frequency Voltage Attenuation in an Electric-Pulse-Excited Stroboscopic Transmission Electron Microscope. *Microsc Microanal* **31**, ozae132 (2025).

We have also provided an explanation for the observed delocalization effect in the TEM images:

Revised manuscript:

Lines 113-121:

Notably, some blurry boundaries in these TEM images are attributed to the delocalization effect[37], which commonly occurs in bright-field TEM imaging, especially under underfocused conditions. In our in situ experiments, the nanotip gradually developed a slight downward tilt by its own weight during prolonged field-emission treatment, which caused additional defocus, thereby enhancing blurriness of the boundaries. This can be mitigated during the observation periods by careful adjustment of the tip height. Although electron-beam delocalization may cause a certain degree of image blurring, the comparison of the nanotip at different time intervals clearly reveals distinct morphological changes that may result from several physical processes triggered by combination of the applied field and the field emission process.

4. Beam-induced hydrocarbon contamination is a known challenge in TEM and can significantly alter surface diffusion and displacement dynamics. It is not clear whether the authors took any measures to prevent or assess contamination. How was surface cleanliness ensured prior to and during the experiments? A discussion of potential contamination effects is necessary given their possible influence on surface-mediated processes.

Response:

Thank you for your valuable comment. We would like to draw the reviewer's attention to the fact that as stated in the manuscript the tungsten nanotips were prepared using an ex situ double-electrolyte electrochemical etching method followed by an in situ Joule melting process. After the first step, an unavoidable oxide layer of a few nanometers had formed on the nanotip surface (see the middle layer in Figure R4). After the second in situ step, the surface was freshly produced in high vacuum (10^{-5} Pa) and naturally appeared free of contaminants, with rounded and smooth apexes, well-ordered lattices containing few internal defects, and a <110> crystallographic direction parallel to the emitter axis.

Secondly, the vacuum level in TEM is sufficiently high (~10^{-5} Pa), and no obvious amorphous carbon layer was observed throughout the entire morphological evolution process even over several hours (Fig. 2) — in contrast to our earlier SEM observations at high magnification, where pronounced amorphous carbon deposition occurred in few seconds, as shown in Figure R3. The corresponding TEM image and EDS line scan results for a nanotip after SEM characterization are shown in Figure R4, revealing a layered structure from the outside to the inside consisting of a carbon layer, an oxide layer, and the tungsten core.

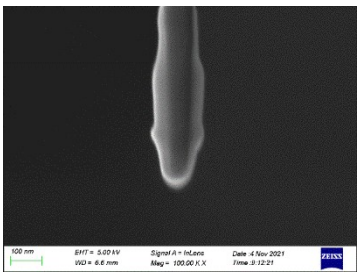

Figure R3. The tungsten nanotip (prepared by the double-electrolyte electrochemical etching method) in SEM covered by an amorphous carbon layer formed via beam-induced hydrocarbon contamination

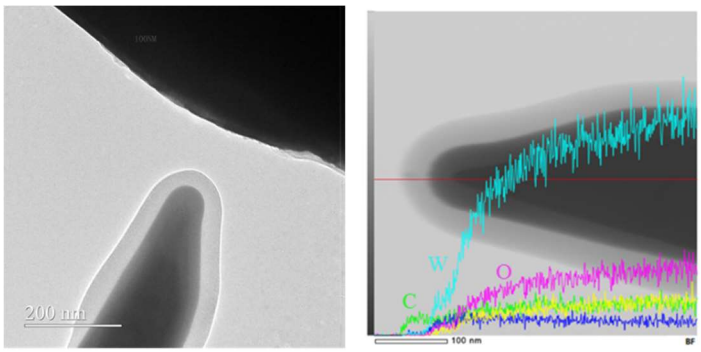

Figure R4. TEM image of the tungsten nanotip (prepared by ex situ double-electrolyte electrochemical etching, during which an oxide layer was introduced) after SEM characterization (which resulted in the deposition of a carbon layer), together with the corresponding EDS line scan acquired along the tip axis.

Thirdly, the field-emission characteristics remained relatively stable, without noticeable fluctuations (see Supplementary Fig. 2 and Supplementary Fig. 5), unlike our previous observation of fluctuating field-emission behavior in a carbon-coated tungsten nanotip [Meng et al., *Phys Rev Lett* **132**, 176201, 2024]. Moreover, the continuous field emission from the nanotip, which also serves as an electron source, likely contributed to in situ cleaning of the tip surface [de Parga *et al.*, *Phys. Rev. Lett.* 80, 357–360, 1998; Feenstra *et al.*, *Surf. Sci.* 181, 295–306, 1987], further suppressing hydrocarbon deposition.

Finally, the electron beam used for imaging was extremely weak (~4 pA/cm^2). In our reverse-polarity experiments without field emission treatment, no carbon layer deposition was observed even several hours (Fig. 4), confirming that beam-induced contamination was negligible under our experimental conditions.

We have added the discussion about the beam-induced hydrocarbon contamination in the revised manuscript and Supplementary Information:

Revised manuscript:

Lines 371-374:

The high vacuum level (~10^{-5} Pa), low beam current density (~4 pA/cm^2) and relatively high field emission current density (which helps to clean the tip surface) render beam-induced hydrocarbon contamination negligible[58,59].

58. de Parga, A. L. V., Hernan, O. S., Miranda, R., Yeyati, A. L., Mingo, N., Martin-Rodero, A., Flores, F. Electron resonances in sharp tips and their role in tunneling spectroscopy. *Phys Rev Lett* **80**, 357-360 (1998).
59. Feenstra, R. M., Stroscio, J. A., Fein, A. P. Tunneling Spectroscopy of the Si(111)2x1 Surface. *Surf Sci* **181**, 295-306 (1987).

Supplementary Information:

Lines 199-215:

(iv) It is also known that the beam-induced hydrocarbon contamination may occur during the TEM imaging[3], however, no obvious amorphous carbon layer was observed during several hours of morphological evolution (~10^{-5} Pa vacuum level in TEM) (Fig. 2 and Fig. 4), in contrast to our earlier SEM observations at high magnification (Supplementary Fig. 21), where pronounced amorphous carbon deposition occurred within seconds. Moreover, during field emission, the field-emission characteristics remained relatively stable, without noticeable fluctuations (see Supplementary Fig. 2 and Supplementary Fig. 5), unlike our previous observation of fluctuating field-emission behavior in a carbon-coated tungsten nanotip[8]. Since the tungsten tip acts as an electron source during field emission, the high current density can even help to clean the tip surface[9,10]. Therefore, we can state with the confidence that the effects of the imaging electron beam are insignificant for the morphology evolution observed in our experiments.

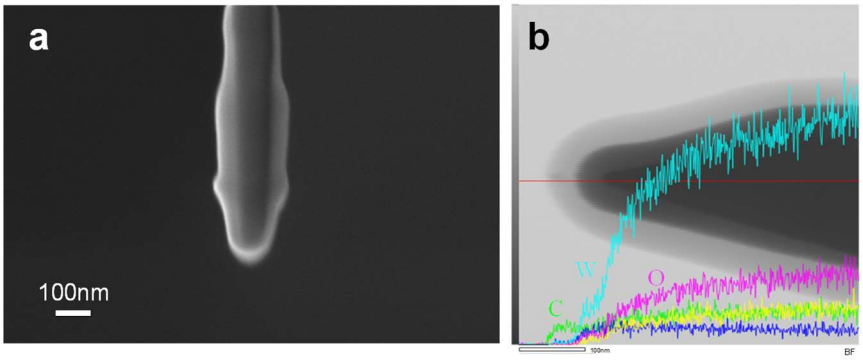

Supplementary Fig. 21| The tungsten nanotip covered by an amorphous carbon layer. (a) The tungsten nanotip (prepared by the double-electrolyte electrochemical etching method) in SEM covered by an amorphous carbon layer formed via beam-induced hydrocarbon contamination. (b) The corresponding EDS line scan along the axis of representative nanotip covered by an amorphous carbon layer.

8. Meng, G., Li, Y., Koitermaa, R. A., Zadin, V., Cheng, Y., Kyritsakis, A. In Situ Observation of Field-Induced Nanoprotrusion Growth on a Carbon-Coated Tungsten Nanotip. *Phys Rev Lett* **132**, 176201 (2024).
9. de Parga, A. L. V., Hernan, O. S., Miranda, R., Yeyati, A. L., Mingo, N., Martin-Rodero, A., Flores, F. Electron resonances in sharp tips and their role in tunneling spectroscopy. *Phys Rev Lett* **80**, 357-360 (1998).
10. Feenstra, R. M., Stroscio, J. A., Fein, A. P. Tunneling Spectroscopy of the Si(111)2x1 Surface. *Surf Sci* **181**, 295-306 (1987).

5. The modeling section lacks important details. It is assumed that an Embedded Atom Method (EAM) potential was used (as mentioned in the reference) in the FEcMD simulations, but the specific interatomic potentials, parameters, and their validation (especially with respect to surface energies and diffusion properties) are not described. Were the potentials tested against experimental or higher-level theoretical data for tungsten? This information is essential to assess the reliability of the simulation results.

Response:

Thank you for your comment. We have not given specific details of the simulations as it was not feasible to produce the complete simulation of the morphological evolution of the nanotips due to a substantial mismatch in accessible timescales (experiments span minutes to hours, while MD simulations are limited to picoseconds to nanoseconds), and the lack of the electron wind force effect in the current model. Simply increasing the applied voltage in simulations to accelerate the evolution is not a viable option, as this would also raise the field emission current, resulting in significant temperature increases and potentially driving the system toward thermal runaway [Kyritsakis *et al.*, *J. Phys. D: Appl. Phys.* **51**, 225203 (2018)], which is clearly beyond the scope of the present experimental conditions. Thus, based on the lattice parameters of tungsten and the experimentally observed crystallographic orientations, we only created an illustrative model of the tip using the MD module in FEcMD. The temperature rise due to Joule heating and Nottingham effects was simulated exclusively with the FEM, HC, and ED modules of FEcMD, without involving the MD module. We have clarified this point in the revised manuscript.

Revised manuscript:

Lines 98-101:

To assist the identification of the crystallographic orientation of the surface facets at the nanotip apex, an illustrative atomistic model is constructed using molecular dynamics (MD) module in field emission coupled with molecular dynamics (FEcMD) computational tool (see Methods section)

Lines 497-527:

Field emission coupled with molecular dynamics (FEcMD)[36] is a multi-scale and multi-physics numerical simulation software package specifically developed to model the complex physical processes occurring in metal nanoelectrodes under strong electric fields. FEcMD consists of four core computational modules: the Molecular Dynamics (MD) module, the Atomic Force (AF) module, the Electrodynamics (ED) module, and the Heat Conduction (HC) module, which are dynamically coupled via the finite element method (FEM). In this study, the MD module is used only to construct tungsten nanotip models with different apex radii. No equilibration of the structure within any given potential was attempted since no atomic dynamics was presently studied. We note that the full MD simulations will require increased values of the applied voltage to observe atomic dynamics within the short MD timespan. High electric fields will inevitably increase field emission currents driving the system to the thermal runaway process[20], which is beyond the scope of the present experimental conditions. Instead, we focused on the analysis of the temperature increase in the tip, which was calculated for every geometry using FEcMD setup (using only the FEM, HC, and ED modules).

In a typical FEcMD setup, each nanotip is divided into an upper atomistic region and a

lower coarse-grained region, to complete the whole emitter geometry, while the coarse grained bottom slab is served as a thermal reservoir in heat conduction calculations, as shown in Supplementary Fig. 7a. For the 2, 3, 5, and 9 nm nanotips, the geometrical parameters are defined as follows. The mushroom cap radii are R = 2, 3, 5, and 9 nm, with corresponding cone top radii of r = 1.4, 2.7, 3, and 7.5 nm. The half-angles of the conic geometry are $\theta = 5°$ for the 2 nm nanotip and $\theta = 10°$ for the others. The MD heights are h = 50, 40, 40, and 30 nm, respectively, while the gap distance is fixed at d = 15 nm. The total tip height above the substrate (including the upper atomistic region and the lower coarse-grained region) is set to H = 100, 80, 80, and 70 nm. These heights are chosen to minimize the effect of H on the electric field while improving computational efficiency. All nanotip models are oriented along the <110> axis, with the crystallographic facets at the apex clearly identified, and the upper atomistic region shown in Fig. 1l, Fig. 2n, Fig. 3h and Fig. 4l for each case. Based on these spherical configuration, the corresponding polyhedral tip structures are obtained by removing selected atoms from the surface planes at the apex of the sphere-cone model.

Moreover, based on the established tip models and using only the FEM, HC, and ED modules, we access the thermal effects for the three fixed tungsten nanotips induced by a field emission current of 1000 nA, with the results detailed in Supplementary Note 3.

20. Kyritsakis, A., Veske, M., Eimre, K., Zadin, V., Djurabekova, F. Thermal runaway of metal nano-tips during intense electron emission. *J Phys D Appl Phys* **51**, 225203 (2018).

Supplementary Information:

Lines 44-46:

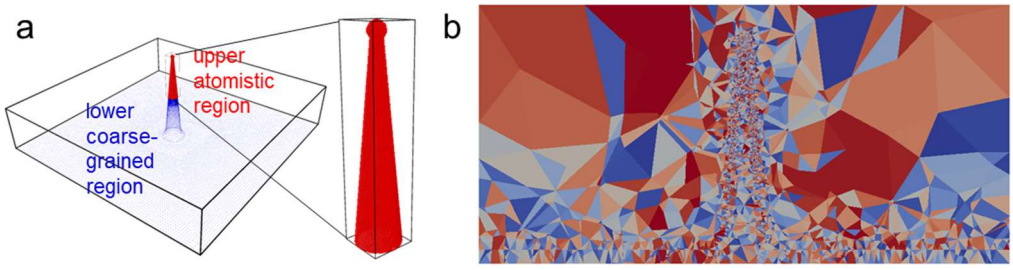

Supplementary Fig. 7| The typical nanotip model in FEcMD simulation. (a) The nanotip model. (b) The finite element mesh.

6. The illustrations labeled as "MD model" (e.g. Figure 1j, Figure 2n or figure 3l) are not clearly explained. They do not appear to be atomistic models, but rather resemble finite element method (FEM) grids? If this is the case, this should be explicitly stated. What physical quantities are being depicted, and at which simulation parameter and time point these models correspond. The relationship between these models and the experimental observations also remains unclear.

Response:

Thank you for your comment. We have clarified the atomistic models in the revised manuscript (see our response to Comment 5). The atomistic modeling was applied to the extent feasible with current state-of-the-art approaches. The model allowed us to estimate that any temperature rise caused by

the field emission currents measured experimentally is negligible. Moreover, it enabled us to observe the facet structures on the surface with the crystallographic orientations used in the experiment.

7. Given that atomistic models have already been generated through MD simulations, the authors should consider performing multislice image simulations. This would enable a direct and quantitative comparison between experimental TEM images and simulated structures, providing stronger support for their interpretations and enhancing the overall impact and rigor of the study.

Response:

Thank you for your professional comment. We have conducted multislice image simulations for a tungsten sphere with an apex radius of 5 nm, both with and without dislocations. The simulated images are consistent with the FFT-filtered TEM images, thereby providing a direct comparison that strengthens the accuracy of the observed dislocation signatures and supports our interpretations. The details are provided in the Supplementary Note 5.

Revised manuscript:

Lines 362-367:

It should be noted that all TEM images are acquired using a JEOL JEM-2100F without spherical aberration (Cs) correction. We have additionally conducted multislice image simulations[56] (see Supplementary Note 5) and confirmed that the spherical aberration values do not significantly affect the images in our experiments; the dislocations observed in the FFT-filtered images are reliable; although the number of dislocations obtained from the FFT-filtered images is lower than the actual number in the nanotip, this does not affect our main conclusions.

56. Koch, C. T. Determination of core structure periodicity and point defect density along dislocations.). Arizona State University (2002).

Supplementary Information:

Lines 140-169:

Supplementary Note 5: Multislice image simulation

The TEM images are simulated using QSTEM software with the multislice method[2]. Two 5 nm tungsten sphere atomistic models are constructed, without or with dislocations, with the ideal zone axis along <100>, as shown in Supplementary Fig. 19a and Supplementary Fig. 20a-b. In practice, however, the TEM holder is a single-tilt TEM holder, making it difficult to perfectly align with the zone axis, resulting in a few degrees of deviation. In our simulations, the imaging direction is set with a 7° tilt from the <100> zone axis. The probe array is set to 500 × 500 pixels, with an imaging resolution of 0.274 × 0.246 Å. In the slicing, the number of slices per sub-slab is 200. The microscope parameters are: high voltage 200 kV, defocus 50 nm, and spherical aberration C_3 = 3 mm and 0 mm. The simulated results are shown in Supplementary Fig. 19b-c and Supplementary Fig. 20c-d. As shown, for the model without dislocations, the simulated images are consistent with the FFT-filtered image in Supplementary Fig. 19d (Fig. 2a), and the spherical aberration values do not significantly affect the imaging. For the model with dislocations, the

simulated images are consistent with the FFT-filtered images with dislocations in Supplementary Fig. 20e (Fig. 2b), and the spherical aberration values also do not significantly affect the imaging. Although the number of dislocations observed from the FFT-filtered images is lower than the actual number in the nanotip, this does not affect our main conclusions.

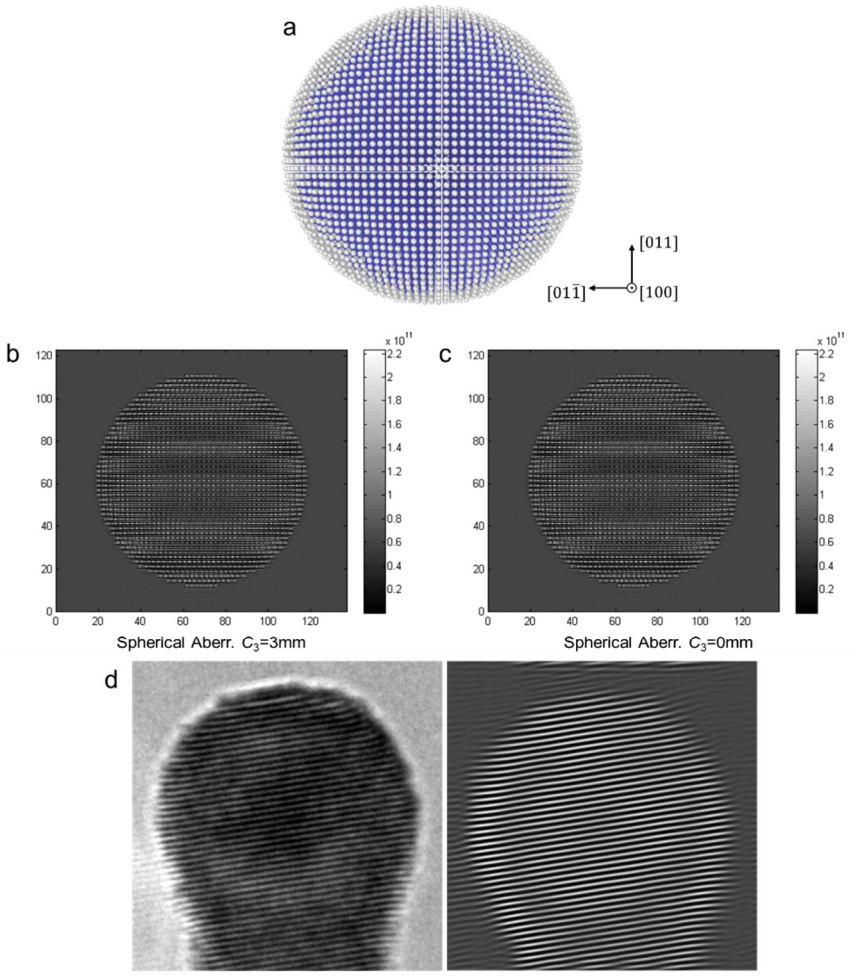

Supplementary Fig. 19| Multislice simulation results of a 5 nm tungsten sphere without dislocations. (a) The atomistic model. (b) Simulated TEM image under spherical aberration with C_3 = 3 mm. (c) Simulated TEM image under spherical aberration with C_3 = 0 mm. (d) TEM image of a 5 nm tungsten nanotip without dislocations, along with the corresponding Fourier-filtered image.

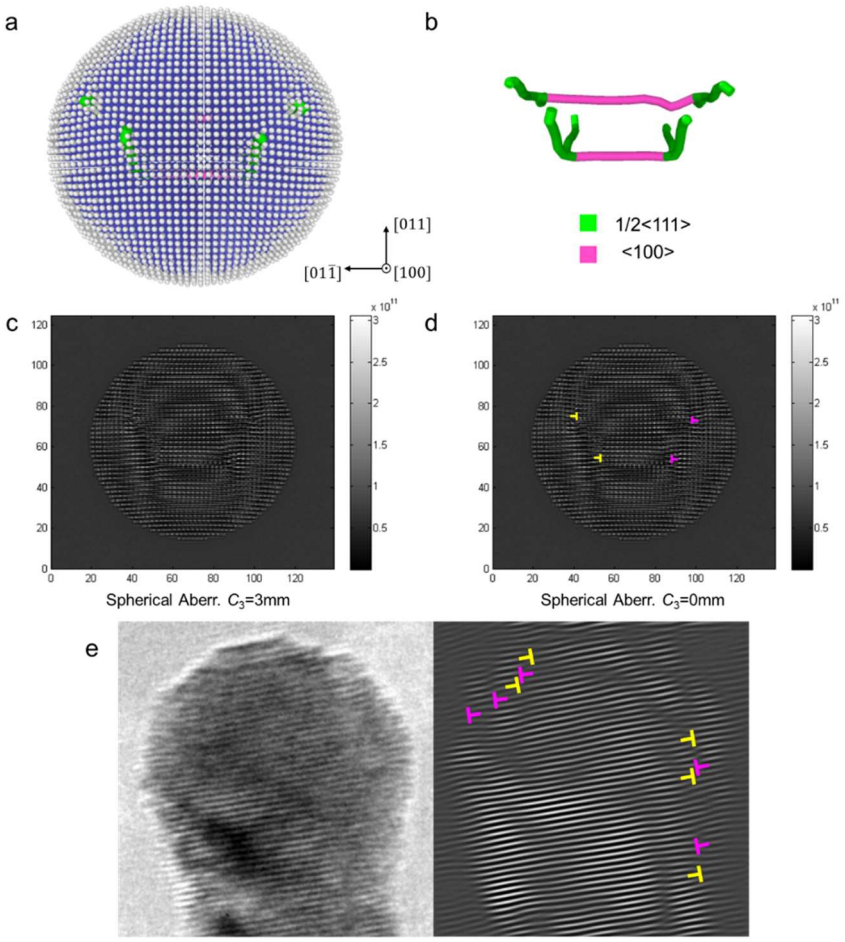

Supplementary Fig. 20| Multislice simulation results of a 5 nm tungsten sphere with dislocations. (a) The atomistic model. (b) The dislocations in the model. (c) Simulated TEM image under spherical aberration with C_3 = 3 mm. (d) Simulated TEM image under spherical aberration with C_3 = 0 mm. (e) TEM image of a 5 nm tungsten nanotip with dislocations, along with the corresponding Fourier-filtered image.

2. Koch, C. T. Determination of core structure periodicity and point defect density along dislocations.). Arizona State University (2002).

8. The authors claim (line 96) that the simulations provide deeper insight into the evolution process, but the specific insights gained are not well articulated. From the supplementary information (Figures 8–10), it seems the simulations mainly serve to rule out thermal effects. If the simulations are intended only for this purpose, that should be clarified. If they offer further structural or morphological insights, those should be clearly presented and discussed.

Response:

As we responded to the Comment 5, the actual MD simulations are not easy to perform, and with current state-of-the-art approaches, the simulations may be rather misleading than clarifying. Therefore, we chose to focus on presenting our experimental observations while continuing to improve the modeling methods. This has been clarified in the revised manuscript.

Revised manuscript:

Lines 502-510:

In this study, the MD module is used only to construct tungsten nanotip models with different apex radii. No equilibration of the structure within any given potential was attempted since no atomic dynamics was presently studied. We note that the full MD simulations will require increased values of the applied voltage to observe atomic dynamics within the short MD timespan. High electric fields will inevitably increase field emission currents driving the system to the thermal runaway process[20], which is beyond the scope of the present experimental conditions. Instead, we focused on the analysis of the temperature increase in the tip, which was calculated for every geometry using FEcMD setup (using only the FEM, HC, and ED modules).

20. Kyritsakis, A., Veske, M., Eimre, K., Zadin, V., Djurabekova, F. Thermal runaway of metal nano-tips during intense electron emission. *J Phys D Appl Phys* **51**, 225203 (2018).

9. A schematic of the experimental geometry is included only in the supplementary material. Given its importance for understanding the local electric field distribution and overall setup, it should be moved to the main manuscript, preferably as part of Figure 1. This will aid readers in contextualizing the results.

Response:

Thank you for your comment. We have included the schematic of the experimental geometry in Figure 1 of the revised manuscript.

Revised manuscript:

Lines 86-87:

Figure 1a-b shows the in situ electrically biased TEM holder and the schematic diagram of the experimental system.

Lines 130-139:

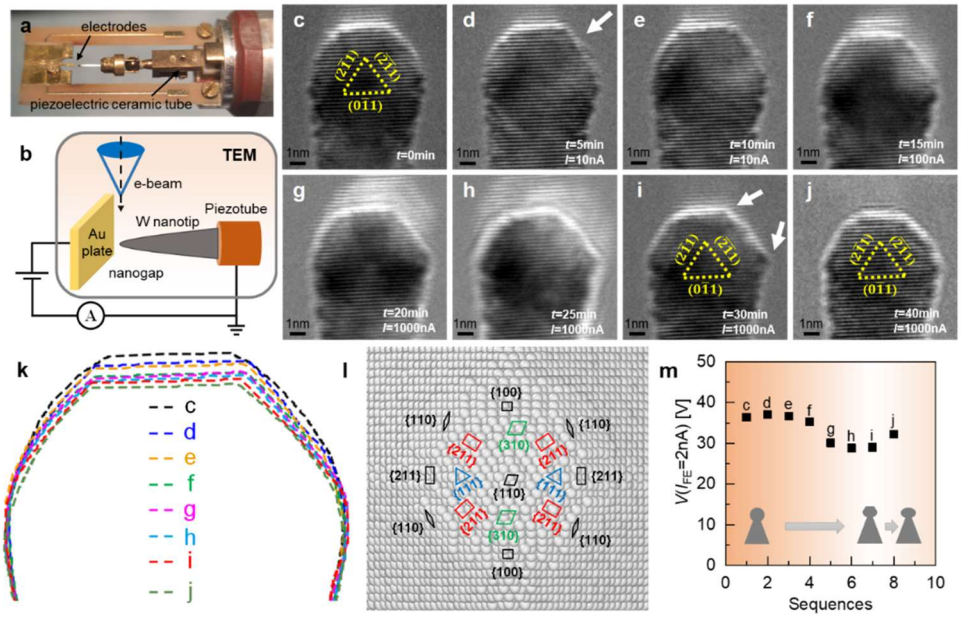

Fig. 1 a The in situ electrically biased TEM holder. **b** The schematic diagram of the in situ

electrical measurement and micromorphology characterization system. **c-j** TEM images showing the progressive deformation behaviors of a <110>-oriented tungsten nanotip with an apex radius of 3 nm during field emission. The corresponding field emission current (I_{FE}) and the cumulative treatment time (t) are indicated in the lower right corner of each image. **k** The surface profiles of tungsten nanotips. **l** The top view of an atomistic model illustrating a <110>-oriented tungsten nanotip with an apex radius of 3 nm. **m** The applied voltages required to achieve a field emission current of 2 nA (d = 15 nm) is plotted in relation to the morphology changes of this tungsten nanotip.

Lines 461-462:

The morphology evolution experiment of pure tungsten nanotips is composed of two periods, the "treatment" period and the "observation" period, as shown in Supplementary Fig. 2.

Supplementary Information:

Lines 18-19:

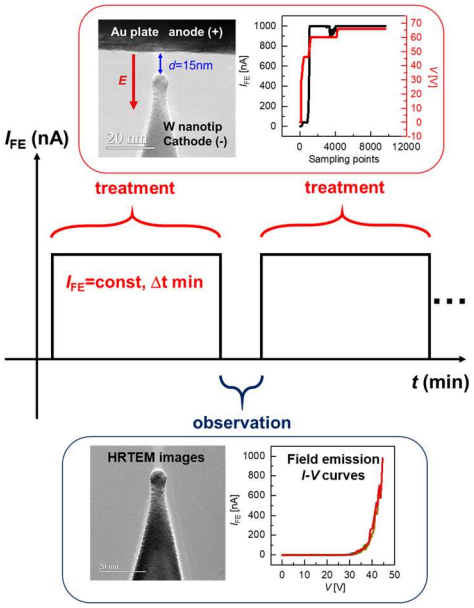

Supplementary Fig. 2| The experimental process for tracking deformation behaviors.

10. The rationale behind the selection of emission currents and treatment times for the different tip radii appears arbitrary and inconsistent. Clarification on how these parameters were chosen and how they allow for direct comparisons between different experimental conditions and tip radii would improve clarity.

Response:

Thank you for your comment. The emission currents and treatment times for different tip radii are determined with the primary goal of capturing the entire morphological evolution process. An initial low-current stage (10 nA for 5-10 minutes) is applied to each tip to observe whether morphological evolution occurs under the initial low field-emission conditions. The 3 nm tip readily evolves even at low currents, whereas the 5 nm and 9 nm tips show negligible changes during this short period (see Figure R5 and Figure R6), which can be neglected compared with the subsequent high-current

stage.

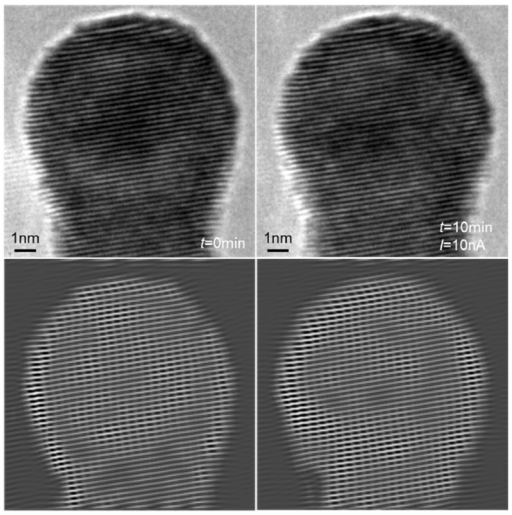

Figure R5. The 5 nm tip morphology before and after 10 nA field emission current treatment

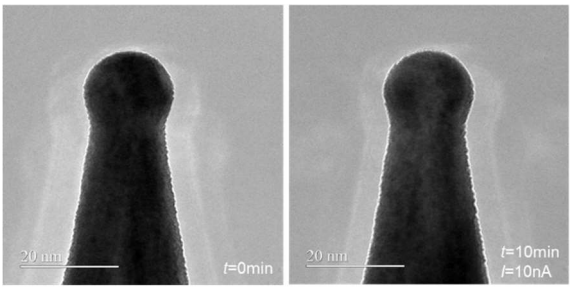

Figure R6. The 9 nm tip morphology before and after 10 nA field emission current treatment

To accelerate and monitor their evolution, the emission current is then increased, with the maximum limit of 1000 nA to avoid a significantly higher breakdown probability at larger currents. The treatment duration for each tip is further refined through in situ TEM observations of tip deformation. Although the imaging resolution is limited (Supplementary Video 1), this real-time monitoring allows tracking of the evolution and timely adjustment of the parameters.

Due to nanosize effects and slight differences in current density, tips with different curvature radii evolve at different rates. The parameters are therefore tailored to capture the entire deformation process, which is essential for comparing the deformation behaviors of different tips.

We have clarified this in the revised manuscript:

Revised manuscript:

Lines 462-482:

During the treatment period, which lasts Δt, the applied voltage is adjusted to maintain a constant field emission current I_{FE} from the tungsten nanotip without any external heating. The morphology of nanotip gradually changes during this treatment period. Notably, the emission currents and treatment times for different tip radii are determined with the primary goal of capturing the entire morphological evolution process. Each experiment begins with an initial low-current stage (10 nA for 5-10 minutes) to observe whether any morphological changes occur under low field-emission conditions. The 3 nm tip readily

evolves even at low currents (Fig. 1), whereas the 5 nm and 9 nm tips show negligible changes in this short period, which can be neglected compared with the subsequent high-current stage (Supplementary Figs. 22-23). To accelerate and monitor their evolution, the emission current is then increased, but limited to the maximum of 1000 nA to avoid an increased electrical breakdown probability at higher currents. The treatment duration for each tip is further refined through in situ TEM observations of tip deformation. Although field emission at 10-13 V/nm slightly reduces imaging resolution, the effect is relatively minor (see Supplementary Video 1). This can be attributed to the slight defocus condition (-50 to -100 nm) in our experiments[60], and the negligible charge accumulation due to the absence of substantial surface contamination (e.g., carbon or oxide, unlike the nanotip in Supplementary Fig. 21)[60]. As a result, real-time monitoring remains effective for tracking the evolution and adjusting parameters. Due to nanosize effects and slight differences in current density, tips with different curvature radii evolve at different rates, so the parameters are therefore tailored to capture the entire deformation process, which is essential for comparing the deformation behaviors of different tips.

60. Zhu, F., Li, W. P., Yeung, M. C., Zhang, Y. X., Du, C. C., Lin, B., Wang, Q., Guo, X. F., Hsueh, Y. C., Chen, F. R., Zhong, X. Y. Quantitative Determination of High-Frequency Voltage Attenuation in an Electric-Pulse-Excited Stroboscopic Transmission Electron Microscope. *Microsc Microanal* **31**, ozae132 (2025).

In conclusion, this manuscript addresses an interesting and timely topic with a unique experimental approach. However, to meet the standards of a high-impact journal, several issues need to be resolved, particularly regarding data interpretation, methodological transparency, and the clarity of both experimental and simulation descriptions. I recommend major revisions to address the points above.

Response:

Thank you again for your positive assessment of our work and we hope that our answers are satisfactorily addressed concerns raised in your review.

Report of Reviewer #3 -- NCOMMS-25-43028 by Yimeng Li et al

Reviewer #3 (Remarks to the Author):

The manuscript investigates the electric-field-induced deformation of tungsten nanotips using in situ transmission electron microscopy (TEM) combined with electrical biasing and modeling. The study provides a direct observation of both surface morphological evolution and internal dislocation dynamics in metallic nanostructures under strong electric fields. The insights are of interest for understanding damage mechanisms in nanoscale field-emission-based electronic devices.
In particular, the authors identify a size-dependent field-assisted evaporation mechanism at field strengths (~10 V/nm) much lower than theoretically expected. The Integration of experiments with ED-MD-PIC simulations adds support to the physical interpretation. The conclusions have implications for nanoelectronics device reliability and design.

Response:

We sincerely appreciate the time and effort you devoted to reviewing our manuscript and providing professional comments. Your suggestions have been extremely valuable in improving the quality of our work. We have carefully addressed each comment and made detailed revisions accordingly. We hope that our explanations and the revised manuscript satisfactorily clarify the issues raised.

In the following, my point-to-point comments for improvement or clarification:

1. The manuscript does not mention the use of spherical aberration (Cs) correction in the images. As the analysis includes lattice-resolved dislocation imaging and shape evolution at the sub-nanometer scale, this raises concerns about the resolution limit and image delocalization artifacts. Delocalization seems strong in the HRTEM panels in Figs 1-4. Could the authors clarify whether any OL Cs correction was used, and if not, discuss the possible limitations of interpreting dislocations dynamics and fine surface features from their HRTEM?

Response:

Thank you for your professional comment. All HRTEM images in this study were acquired using a JEOL JEM-2100F microscope operated at 200 kV without objective-lens spherical aberration (Cs) correction. This setup provides a point resolution of 0.23 nm and a line resolution of 0.10 nm, which are sufficient to resolve the (110) lattice fringes of tungsten (d = 0.223 nm) and to identify associated line defects such as dislocations. In our experiments, although the ideal zone axis for the 5 nm nanotip is along <100>, in practice, the use of a single-tilt TEM holder makes perfect alignment with the zone axis difficult, resulting in a few degrees of deviation. Due to this imaging direction and the maximum tip thickness of approximately 10 nm, atoms from different layers are slightly misaligned in projection. As a result, individual atoms within the plane cannot be distinguished and instead appear as continuous lattice fringes.

We acknowledge that, without Cs correction, fine surface atomic features and the precise cores

of dislocations may not be fully resolved [Zhou et al., Crit. Rev. Solid State Mater. Sci. 47, 388, 2022]. Image contrast can be influenced by the non-uniform thickness of the nanotip and the disrupted lattice fringes may originate from overlapping dislocations [Wang et al., Nat. Commun. 11, 2497 (2020)], as their inherently three-dimensional structures are projected into a two-dimensional image [Bilyk et al., Sci. Rep. 14, 25168, 2024]. As a result, the actual defect configurations can be more complex than what is directly observed in TEM images or inferred from FFT-filtered images. To address this, multislice simulations have been performed, confirming that variations in spherical aberration values have only a minor effect on the images under our experimental conditions; the dislocations observed in the FFT-filtered images are reliable; although the number of dislocations obtained from the FFT-filtered images is lower than the actual number in the nanotip, this does not affect our main conclusions. The details are provided in the Supplementary Note 5

We have included this discussion in the revised manuscript and Supplementary Information:

Revised manuscript:

Lines 362-367:

It should be noted that all TEM images are acquired using a JEOL JEM-2100F without spherical aberration (Cs) correction. We have additionally conducted multislice image simulations[56] (see Supplementary Note 5) and confirmed that the spherical aberration values do not significantly affect the images in our experiments; the dislocations observed in the FFT-filtered images are reliable; although the number of dislocations obtained from the FFT-filtered images is lower than the actual number in the nanotip, this does not affect our main conclusions.

56. Koch, C. T. Determination of core structure periodicity and point defect density along dislocations.). Arizona State University (2002).

Supplementary Information:

Lines 140-169:

Supplementary Note 5: Multislice image simulation

The TEM images are simulated using QSTEM software with the multislice method[2]. Two 5 nm tungsten sphere atomistic models are constructed, without or with dislocations, with the ideal zone axis along <100>, as shown in Supplementary Fig. 19a and Supplementary Fig. 20a-b. In practice, however, the TEM holder is a single-tilt TEM holder, making it difficult to perfectly align with the zone axis, resulting in a few degrees of deviation. In our simulations, the imaging direction is set with a 7° tilt from the <100> zone axis. The probe array is set to 500 × 500 pixels, with an imaging resolution of 0.274 × 0.246 Å. In the slicing, the number of slices per sub-slab is 200. The microscope parameters are: high voltage 200 kV, defocus 50 nm, and spherical aberration C_3 = 3 mm and 0 mm. The simulated results are shown in Supplementary Fig. 19b-c and Supplementary Fig. 20c-d. As shown, for the model without dislocations, the simulated images are consistent with the FFT-filtered image in Supplementary Fig. 19d (Fig. 2a), and the spherical aberration values do not significantly affect the imaging. For the model with dislocations, the simulated images are consistent with the FFT-filtered images with dislocations in

Supplementary Fig. 20e (Fig. 2b), and the spherical aberration values also do not significantly affect the imaging. Although the number of dislocations observed from the FFT-filtered images is lower than the actual number in the nanotip, this does not affect our main conclusions.

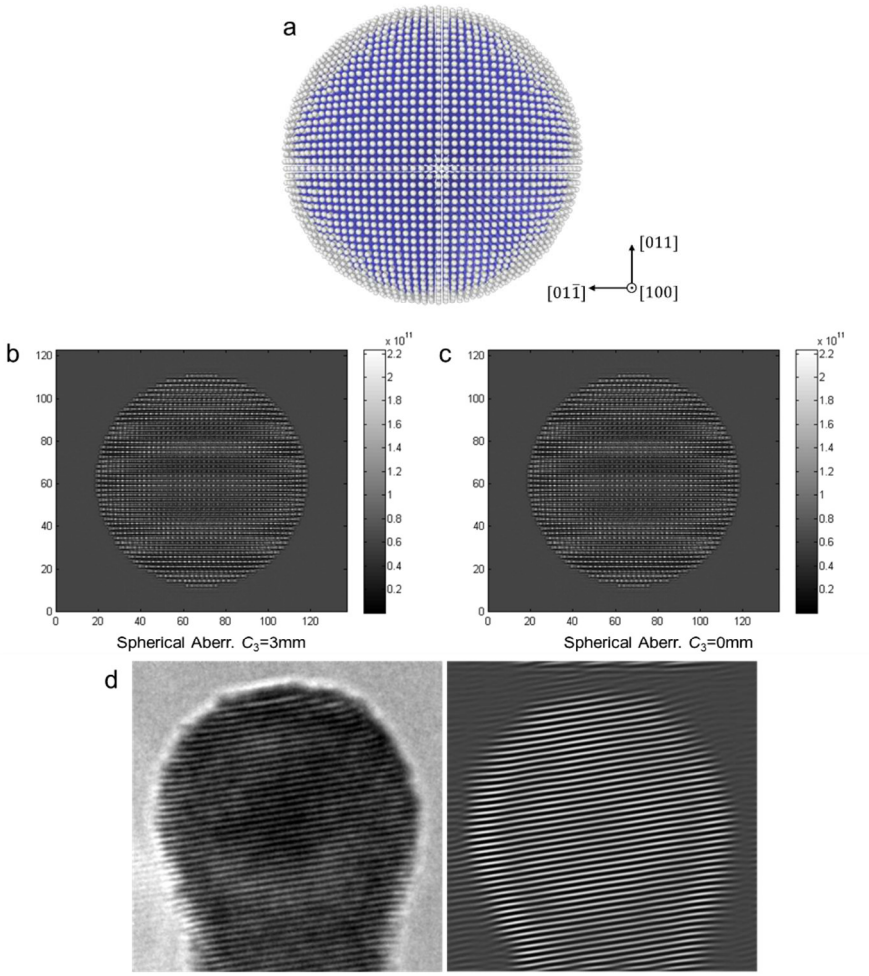

Supplementary Fig. 19| Multislice simulation results of a 5 nm tungsten sphere without dislocations. (a) The atomistic model. (b) Simulated TEM image under spherical aberration with C_3 = 3 mm. (c) Simulated TEM image under spherical aberration with C_3 = 0 mm. (d) TEM image of a 5 nm tungsten nanotip without dislocations, along with the corresponding Fourier-filtered image.

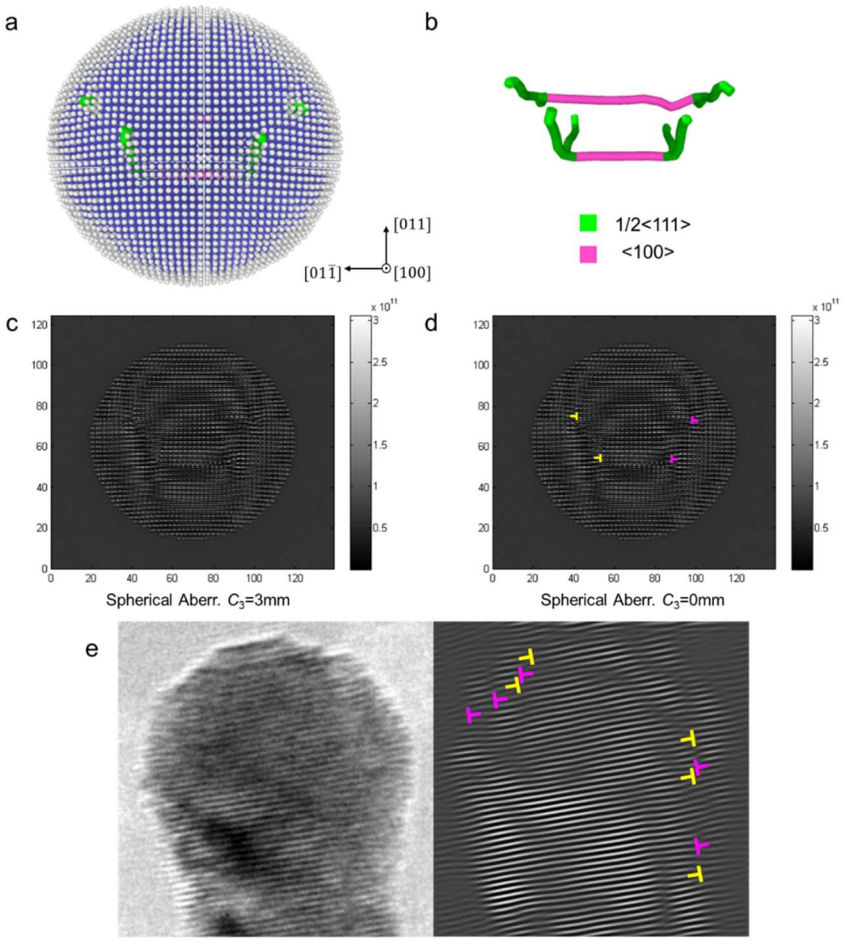

Supplementary Fig. 20| Multislice simulation results of a 5 nm tungsten sphere with dislocations. (a) The atomistic model. (b) The dislocations in the model. (c) Simulated TEM image under spherical aberration with C_3 = 3 mm. (d) Simulated TEM image under spherical aberration with C_3 = 0 mm. (e) TEM image of a 5 nm tungsten nanotip with dislocations, along with the corresponding Fourier-filtered image.

2. Koch, C. T. Determination of core structure periodicity and point defect density along dislocations.). Arizona State University (2002).

In Fig. 1, the slight extension of the fringes beyond the nanotip boundary may result from the delocalization effect, which commonly occurs in bright-field TEM imaging, especially under underfocused conditions. In our in situ experiments, the nanotip gradually developed a slight downward tilt during prolonged field emission treatment—likely due to its own weight—which may have increased the defocus and thereby enhanced this effect. Nevertheless, such an effect can be mitigated during the observation periods by carefully adjusting the tip height. We acknowledge that electron-beam delocalization may introduce a certain degree of image blurring. However, comparison of the nanotip profiles at different time points clearly reveals an unambiguous morphological change. The delocalization effect does not affect the primary conclusions drawn from the TEM images. We have explicitly emphasized this point in the revised manuscript:

Revised manuscript:

Lines 113-121:

Notably, some blurry boundaries in these TEM images are attributed to the delocalization effect[37], which commonly occurs in bright-field TEM imaging, especially under underfocused conditions. In our in situ experiments, the nanotip gradually developed a slight downward tilt by its own weight during prolonged field-emission treatment, which caused additional defocus, thereby enhancing blurriness of the boundaries. This can be mitigated during the observation periods by careful adjustment of the tip height. Although electron-beam delocalization may cause a certain degree of image blurring, the comparison of the nanotip at different time intervals clearly reveals distinct morphological changes that may result from several physical processes triggered by combination of the applied field and the field emission process.

2. Given the reliance on Fourier-filtered images to detect dislocations, I strongly recommend that the authors complement their experimental images with multislice image simulations. These should reproduce the conditions close to the experiment, in particular defocus values and crystallographic orientation. A comparison between simulated images of defect-free tip and tip with dislocations would help validate whether the dislocation contrast observed in the experimental FFT-filtered images is physically meaningful or could be influenced by imaging artifacts. This step would significantly strengthen the interpretation of the internal defect dynamics.

Response:

Thank you for your professional comment. We have conducted multislice image simulations for tungsten spheres with an apex radius of 5 nm, both with and without dislocations, under conditions closely matching the experiments, including defocus values and crystallographic orientation. The simulated images are consistent with the experimental FFT-filtered images, reinforcing the accuracy of the observed dislocation signatures and strengthening the interpretation of internal defect dynamics. The details are provided in the Supplementary Note 5.

Revised manuscript:

Lines 362-367:

It should be noted that all TEM images are acquired using a JEOL JEM-2100F without spherical aberration (Cs) correction. We have additionally conducted multislice image simulations[56] (see Supplementary Note 5) and confirmed that the spherical aberration values do not significantly affect the images in our experiments; the dislocations observed in the FFT-filtered images are reliable; although the number of dislocations obtained from the FFT-filtered images is lower than the actual number in the nanotip, this does not affect our main conclusions.

56. Koch, C. T. Determination of core structure periodicity and point defect density along dislocations.). Arizona State University (2002).

Supplementary Information:

Lines 140-169:

Supplementary Note 5: Multislice image simulation

The TEM images are simulated using QSTEM software with the multislice method[2]. Two 5 nm tungsten sphere atomistic models are constructed, without or with dislocations, with the ideal zone axis along <100>, as shown in Supplementary Fig. 19a and Supplementary Fig. 20a-b. In practice, however, the TEM holder is a single-tilt TEM holder, making it difficult to perfectly align with the zone axis, resulting in a few degrees of deviation. In our simulations, the imaging direction is set with a 7° tilt from the <100> zone axis. The probe array is set to 500 × 500 pixels, with an imaging resolution of 0.274 × 0.246 Å. In the slicing, the number of slices per sub-slab is 200. The microscope parameters are: high voltage 200 kV, defocus 50 nm, and spherical aberration C_3 = 3 mm and 0 mm. The simulated results are shown in Supplementary Fig. 19b-c and Supplementary Fig. 20c-d. As shown, for the model without dislocations, the simulated images are consistent with the FFT-filtered image in Supplementary Fig. 19d (Fig. 2a), and the spherical aberration values do not significantly affect the imaging. For the model with dislocations, the simulated images are consistent with the FFT-filtered images with dislocations in Supplementary Fig. 20e (Fig. 2b), and the spherical aberration values also do not significantly affect the imaging. Although the number of dislocations observed from the FFT-filtered images is lower than the actual number in the nanotip, this does not affect our main conclusions.

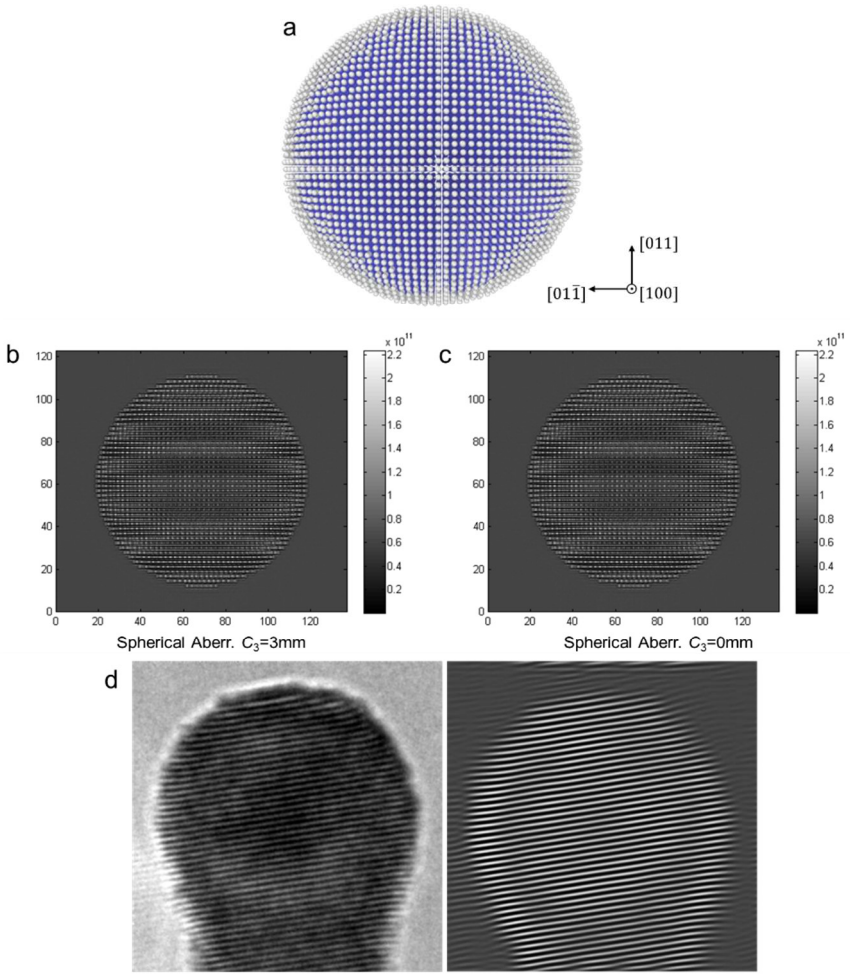

Supplementary Fig. 19| Multislice simulation results of a 5 nm tungsten sphere without dislocations. (a) The atomistic model. (b) Simulated TEM image under spherical aberration with C_3 = 3 mm. (c) Simulated TEM image under spherical aberration with C_3 = 0 mm. (d) TEM image of a 5 nm tungsten nanotip without dislocations, along with the corresponding Fourier-filtered image.

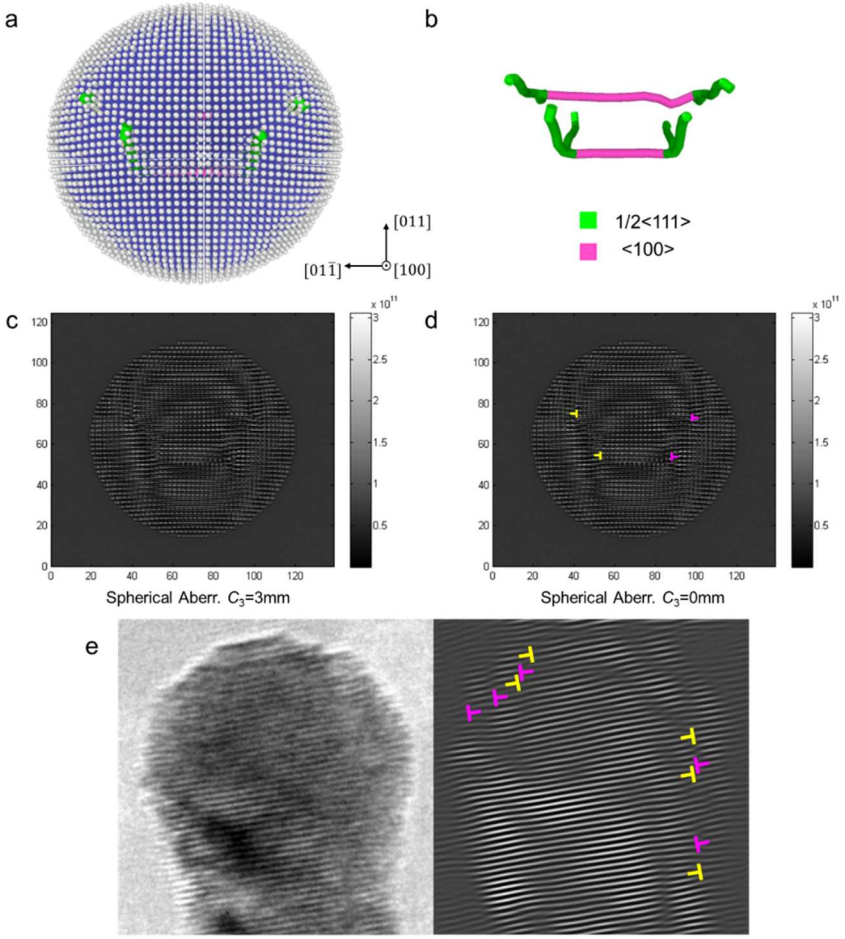

Supplementary Fig. 20| Multislice simulation results of a 5 nm tungsten sphere with dislocations. (a) The atomistic model. (b) The dislocations in the model. (c) Simulated TEM image under spherical aberration with C_3 = 3 mm. (d) Simulated TEM image under spherical aberration with C_3 = 0 mm. (e) TEM image of a 5 nm tungsten nanotip with dislocations, along with the corresponding Fourier-filtered image.

2. Koch, C. T. Determination of core structure periodicity and point defect density along dislocations.). Arizona State University (2002).

3. The estimates for electric field strength, field enhancement factors, and evaporation thresholds would benefit from a more detailed analysis of uncertainty sources, particularly in the simulations. Moreover, did the authors consider the charging of the tip due to the electric field applied? Static charge can accumulate at the surface even in metallic nanostructures and persist after the field is switched off. They contribute to the potential

seen by the beam electrons during imaging in defocus conditions, as for the HRTEM images presented here. The author should discuss about this. Here is a reference in the field that the authors could cite: doi.org/10.1039/D0NR00739K

Response:

Thank you for your comment. The estimates of electric field strength, field enhancement factors, and evaporation thresholds may be influenced by several factors, primarily (i) the atomistic electric field distribution and (ii) the slight differences between real nanotips and the idealized simulated geometries.

Firstly, we have simulated the electric field distribution for atomistic spherical and polyhedral nanotips with apex radii of 2 nm, 3 nm and 5 nm. The electric field distribution was obtained by FEcMD simulation. In FEcMD, the finite element mesh (FEM) generation is supported by the open-source Deal.II library [Veske et al., J. Comput. Phys. 367, 279–294, 2018; Bangerth et al., ACM Trans. Math. Softw. 33, 24, 2007], covering the vacuum region, the surface, and the interior of the electron emitter, especially enabling electric field simulations. The simulated results are shown in Figure R7, Figure R8 and Figure R9. As can be seen, the increase in electric field due to the polyhedral geometry is relatively small. For example, for a nanotip with a 3 nm apex radius, the spherical geometry yields an electric field of 12 V/nm, while the polyhedral geometry increases it slightly to 12.3 V/nm. Similarly, for a 5 nm apex radius, the electric field increases from 10.5 V/nm (spherical) to 10.8 V/nm (polyhedral). Although the increase in electric field is modest, the field emission current of the polyhedral tip is larger than that of the spherical tip under the same applied voltage. This can be attributed to the larger effective emission area of the polyhedral apex. The combined effect of the slightly enhanced electric field and the increased effective emission area leads to a relatively smaller field emission voltage at I_{FE} = 2 nA observed in experiments.

Secondly, the simulated model used here is somewhat idealized, but the difference from realistic structures is not expected to be significant. In our previous work, we have shown that the simulated field enhancement factors agree well with experimental field emission characteristics (see Fig. 2e in [Li et al., Nat. Commun. 16, 5583, 2025]), still capturing the universal scaling relationship for nanoscale field emission, expressed as $\gamma_a \cdot V_m \propto d/R$, where γ_a represents the simulated apex field enhancement factor, V_m denotes the field emission voltage at a specified emission current (e.g., I = 2 nA), d is the gap distance, and R is the apex radius. The field enhancement factors obtained here (Figure R7, Figure R8 and Figure R9) are also consistent with the reported universal relationship between the field enhancement factor and R/d (see Fig. 2d in [Li et al., Nat. Commun. 16, 5583, 2025]). Therefore, an evaporation threshold in the range of 10-13 V/nm can be considered reliable.

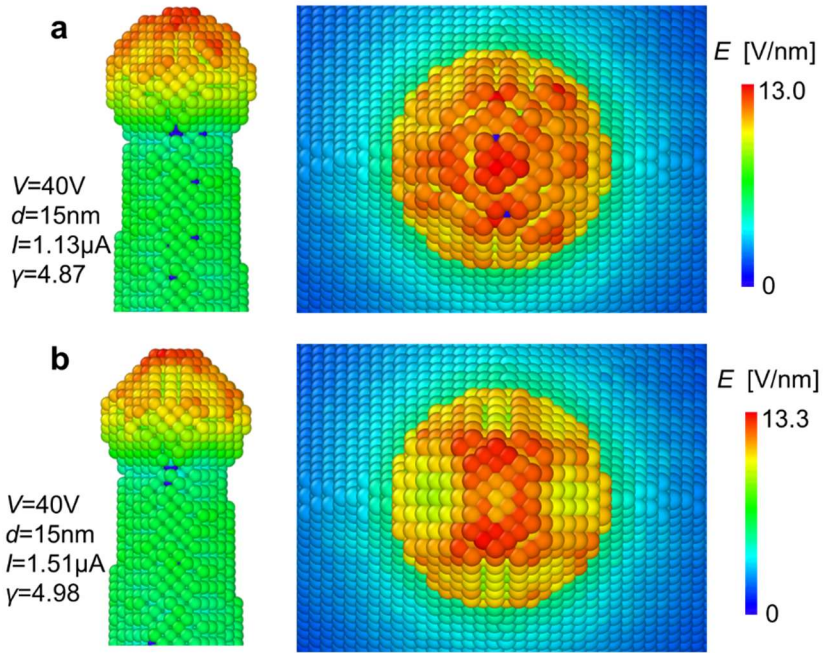

Figure R7. The local electric field distribution for atomistic models: (a) the spherical nanotip and (b) the polyhedral nanotip with a 2 nm apex radius.

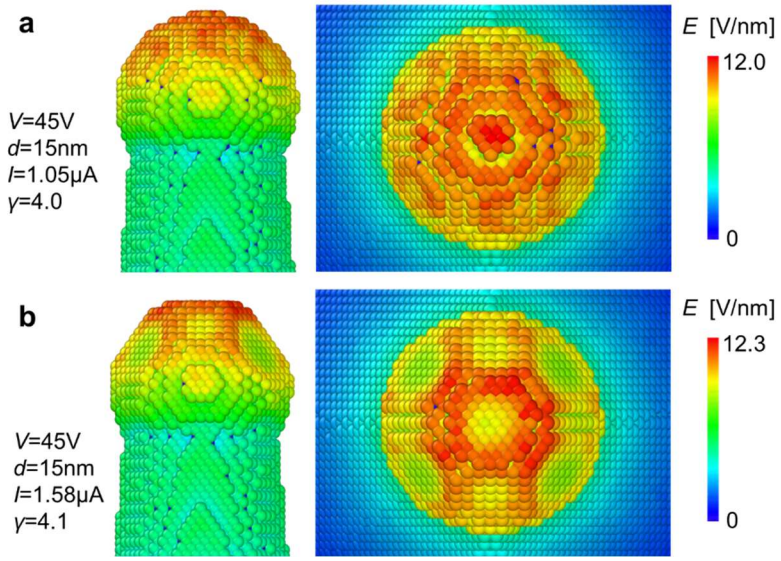

Figure R8. The local electric field distribution for atomistic models: (a) the spherical nanotip and (b) the polyhedral nanotip with a 3 nm apex radius.

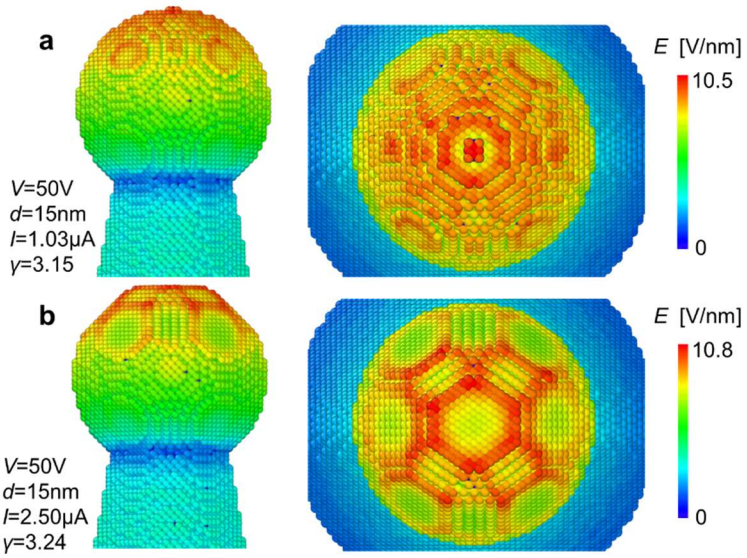

Figure R9. The local electric field distribution for atomistic models: (a) the spherical nanotip and (b) the polyhedral nanotip with a 5 nm apex radius.

We have added the detailed analysis about electric field strength, field enhancement factors, and evaporation thresholds in the revised manuscript and Supplementary Information:

Revised manuscript:

Lines 124-127:

It can be seen that with the deformation of the nanotip into a polyhedral shape, its field emission capability increases, which can be attributed to the combined effects of a slightly enhanced electric field and an enlarged effective emission area, as demonstrated in Supplementary Fig. 8.

Lines 270-277:

The maximum local electric field of 2 nm nanotip is highest among different nanotips and reaches about 13.0 V/nm for spherical shape (Supplementary Fig. 18), with a slight increase (13.3 V/nm) for polyhedral geometry. Although the simulated model is idealized, the differences between simulated models and realistic structures are not significant[39]. It is surprising that atom evaporation in our experiments occurs at the electric field values of 10-13 V/nm (see Supplementary Note 1 and Supplementary Fig. 18) because they are significantly lower than the previously reported thresholds of 40-60 V/nm[40,41].

39. Li, Y. M., Xia, L. H., Li, N., Tang, S. L., Ge, Y. S., Wang, J. Y., Xiao, B., Cheng, Y. H., Ang, L. K., Meng, G. D. Uncovering a widely applicable empirical formula for field emission characteristics of metallic nanotips in nanogaps. *Nat Commun* **16**, 5583 (2025).
40. Golubev, O. L. Experimental determination of evaporating electric field strengths for nanodimensional field ion emitters. *Tech Phys Lett* **40**, 1092-1094 (2014).
41. Ashton, M., Mishra, A., Neugebauer, J., Freysoldt, C. Description of Bond Breaking in Large Electric Fields. *Phys Rev Lett* **124**, 176801 (2020).

Supplementary Information:

Lines 38-56:

Supplementary Note 1: The simulated electric field distribution for atomistic models

Based on the established model (a typical example is shown in Supplementary Fig. 7), the atomically mapped field distributions of spherical and polyhedral nanotips with apex radii of 3 nm, 5 nm, and 9 nm are shown in Supplementary Figs. 8-10. It can be seen that the electric field is stronger at the edge atoms, and the polyhedral nanotips exhibit only a slight increase in field strength compared with the spherical ones.

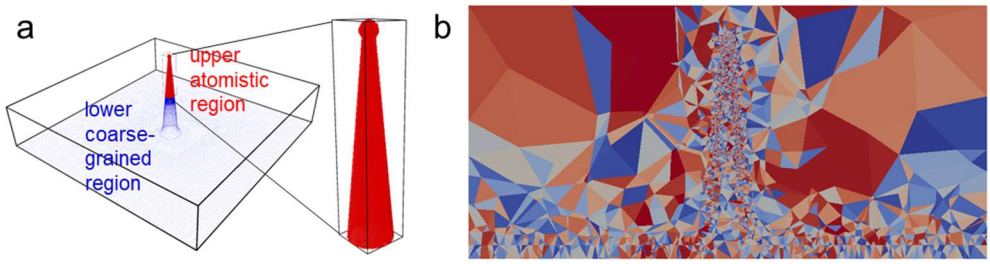

Supplementary Fig. 7| The typical nanotip model in FEcMD simulation. (a) The nanotip model. (b) The finite element mesh.

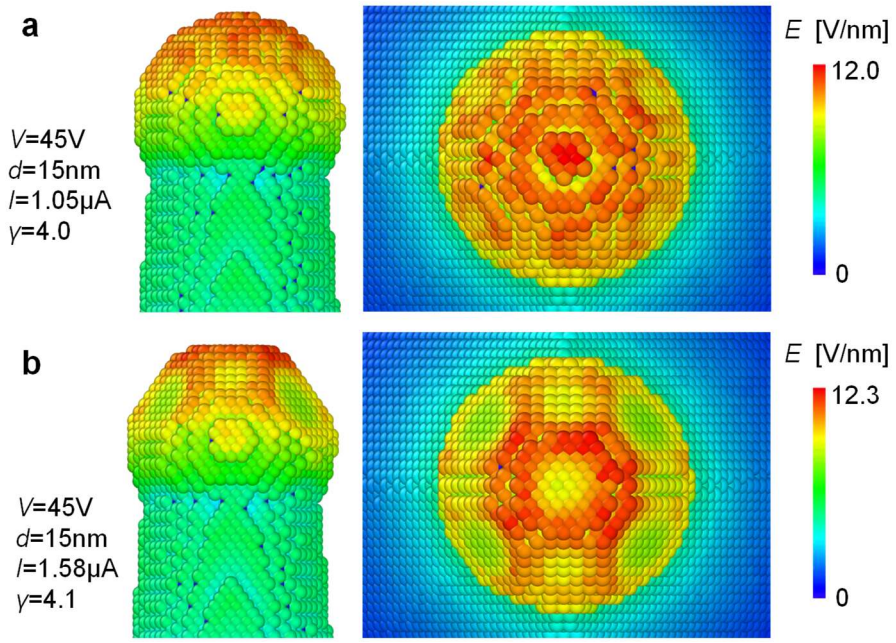

Supplementary Fig. 8| The electric field distribution for the atomistic spherical nanotip and the polyhedral nanotip with a 3 nm apex radius. (a) The spherical nanotip. (b) The polyhedral nanotip.

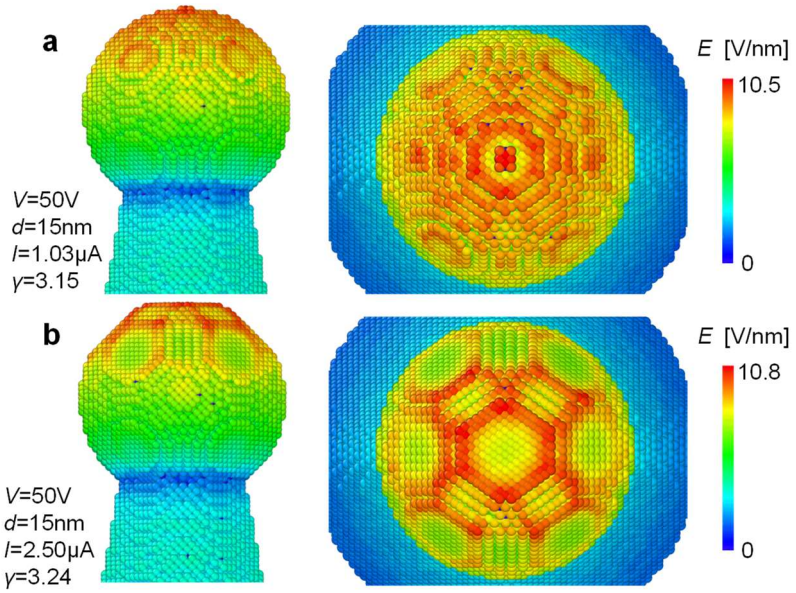

Supplementary Fig. 9| The electric field distribution for the atomistic spherical nanotip and the polyhedral nanotip with a 5 nm apex radius. (a) The spherical nanotip. (b) The polyhedral nanotip.

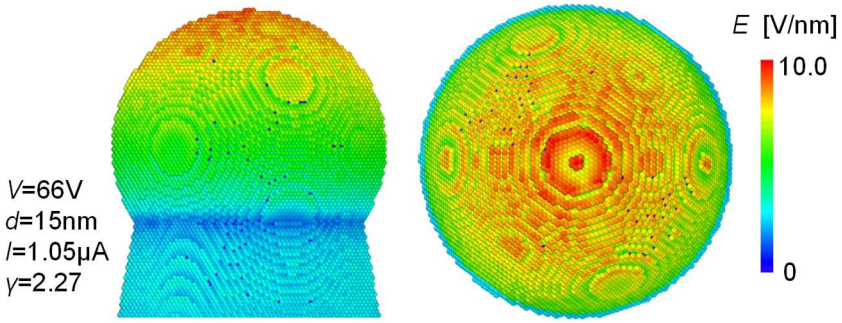

Supplementary Fig. 10| The electric field distribution for the atomistic spherical nanotip with a 9 nm apex radius.

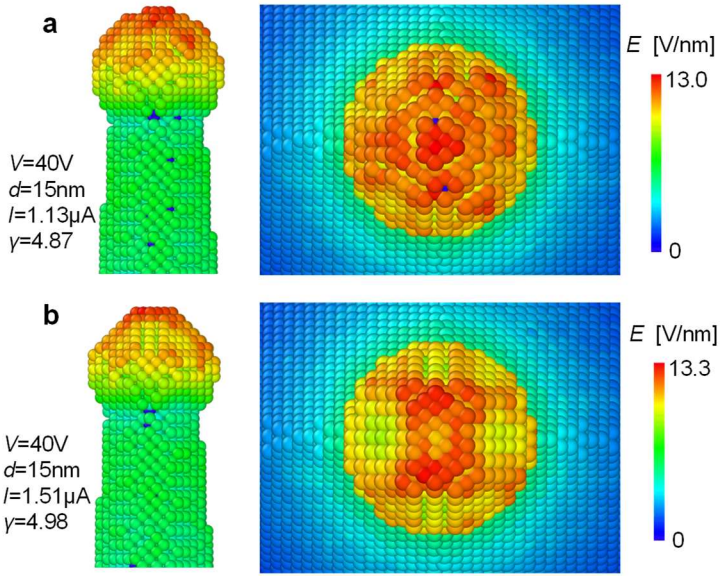

Supplementary Fig. 18| The electric field distribution for the atomistic spherical nanotip and the polyhedral nanotip with a 2 nm apex radius. (a) The spherical nanotip. (b) The polyhedral nanotip.

Regarding the possibility of charge accumulation, we note the following. First, the fabricated nanotips do not exhibit a significant carbon layer or oxide layer (unlike the tungsten nanotip in Supplementary Fig. 21), and our pure tungsten tips, with high conductivity, are always connected to the ground, so noticeable charge accumulation is unlikely. Second, during the observation periods, we continuously acquired HRTEM images and repeatedly measured field emission characteristics. The field-emission *I-V* curves show good reproducibility (see Figure R10), further indicating the absence of measurable charge accumulation. In addition, Zhu *et al.* [Microsc. Microanal. **31**, ozae132 (2025)] reported that when gradually applying voltages from -20 V to +20 V to two tungsten nanotips, no significant charge buildup was observed at 0 V under a maximum defocus of -1 mm, and at 20 V, no significant charge effect was observed when the defocus value was 0. In our experiments, HRTEM imaging was carried out under slightly underfocused conditions (typically in the range of -50 nm to -100 nm); thus, even if residual charges were present, their effect on imaging would be negligible.

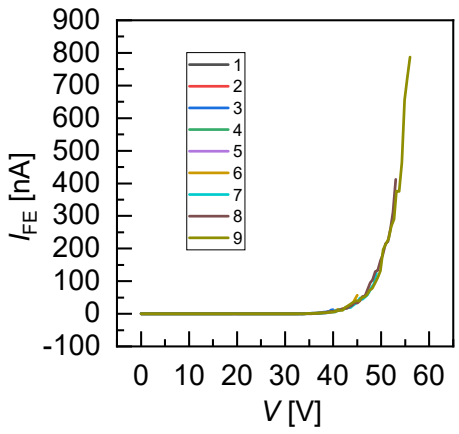

Figure R10 The representative *I-V* curves during one observation period

During voltage application, induced charges are indeed present on both electrodes to establish the electric field, which in principle may influence TEM imaging. However, according to Zhu *et al.* [Microsc. Microanal. **31**, ozae132 (2025)], the effect of induced charges on image is negligible under near-focus or slightly underfocused conditions, and only at strongly underfocused conditions does the influence become significant. The Supplementary Video 1 shows the real-time imaging of 5 nm nanotip during the 1 μA field emission current treatment, where no significant image changes are observed compared to the acquired TEM images during observation periods. It should also be clarified that the stripes observed in Fig. 1 are not caused by induced charges but rather by the delocalization effect in bright-field TEM imaging during the observation periods. In our prolonged in situ experiments, a slight downward drift of the nanotip due to its own weight may have increased the defocus, thereby further enhancing this effect and leading to the blurry boundaries observed in some images. This effect can be mitigated during the observation periods by adjusting the tip height.

We have added this discussion about charge accumulation and delocalization effect in the revised manuscript:

Revised manuscript:

Lines 113-121:

Notably, some blurry boundaries in these TEM images are attributed to the delocalization effect[37], which commonly occurs in bright-field TEM imaging, especially under underfocused conditions. In our in situ experiments, the nanotip gradually developed a slight downward tilt by its own weight during prolonged field-emission treatment, which caused additional defocus, thereby enhancing blurriness of the boundaries. This can be mitigated during the observation periods by careful adjustment of the tip height. Although electron-beam delocalization may cause a certain degree of image blurring, the comparison of the nanotip at different time intervals clearly reveals distinct morphological changes that may result from several physical processes triggered by combination of the applied field and the field emission process.

Lines 474-479:

Although field emission at 10-13 V/nm slightly reduces imaging resolution, the effect is relatively minor (see Supplementary Video 1). This can be attributed to the slight defocus condition (-50 to -100 nm) in our experiments[60], and the negligible charge accumulation due to the absence of substantial surface contamination (e.g., carbon or oxide, unlike the nanotip in Supplementary Fig. 21)[60]. As a result, real-time monitoring remains effective for tracking the evolution and adjusting parameters.

60. Zhu, F., Li, W. P., Yeung, M. C., Zhang, Y. X., Du, C. C., Lin, B., Wang, Q., Guo, X. F., Hsueh, Y. C., Chen, F. R., Zhong, X. Y. Quantitative Determination of High-Frequency Voltage Attenuation in an Electric-Pulse-Excited Stroboscopic Transmission Electron Microscope. *Microsc Microanal* **31**, ozae132 (2025).

4. The observed nucleation and annihilation of dislocations are compelling, but the

authors could elaborate more on whether these processes are surface-driven or related to stress release from atom evaporation.

Response:

Thank you for your comment. In our study, the dislocation nucleation process is largely surface-driven, involving roughness-enhanced electric field stress [Gouldstone et al., Nature 411, 656, 2001], high surface atom free energy (especially at edges) [Ding et al., ACS Nano 18, 4170, 2024], electron-wind-assisted surface atomic displacement [Li et al., Acta Mater. 223, 117461, 2022], and stress redistribution due to surface atom evaporation. The dislocation annihilation process is primarily attributed to the high surface-to-volume ratio of nanotips, where free surfaces act as efficient sinks [Zhu et al., Phys. Rev. Lett. 100, 025502, 2008], and to the formation of dipoles by dislocations of opposite sign [Essmann et al., Philos Mag A 40, 731-756, 1979].

For dislocation nucleation, atom evaporation generates surface steps and edges that increase local roughness. These features have two primary effects: first, they slightly enhance the local electric-field stress, which scales with the square of the field strength (Supplementary Note 2); second, they act as classical stress concentrators, thereby lowering the barrier for dislocation nucleation. As steps and edges grow, their stress-concentration factors increase, eventually driving the local stress above the nucleation threshold. Once near-surface dislocations form, the electron wind is sufficient to drive their propagation from the surface into the bulk, as particularly evident in the comparisons between Fig. 2 and Fig. 4. Moreover, the combined action of the strong electric field and electron wind enhances surface atom migration and evaporation, where ongoing atom evaporation releases and redistributes local stresses in the near-surface lattice, creating new high-stress regions that can trigger further dislocation nucleation.

For dislocation annihilation, the exceptionally high surface-to-volume ratio of the nanotip makes free surfaces highly effective dislocation sinks. The image stress between a dislocation and the free surface invariably drives the dislocation toward annihilation once their separation becomes sufficiently small. Likewise, dislocations of opposite sign can mutually attract, forming dipoles that annihilate when in close proximity. Both the field-induced stress and electron wind force contribute to dislocation mobility, thereby accelerating their annihilation either at the surface or through dipole formation.

We have provided a more detailed discussion of the observed nucleation and annihilation of dislocations in the revised manuscript:

Revised manuscript:

Lines 300-330:

Compared to reverse polarity experiments (Fig. 3 and Fig. 4), the field emission experiments (Fig. 1 and Fig. 2) include electron wind effects. At I_{FE} = 1000 nA, the current densities are approximately 3.54×10^{6} A cm^{-2}, 1.27×10^{6} A cm^{-2} and 3.90×10^{5} A cm^{-2} for tungsten nanotips with apex radii of 3 nm, 5 nm and 9 nm, respectively. Despite the minimal macroscopic temperature rise (remaining around 300 K, see Supplementary Note 3), in regions with local lattice distortions such as dislocations, enhanced electron-phonon scattering leads to a significant electron wind effect, which may locally elevate atomic temperatures at defect sites. For the three nanotips with different apex radii, the estimated

electron wind forces acting on dislocations reach approximately 3.3×10^4 Pa, 1.2×10^4 Pa and 3.7×10^3 Pa[44], indicating that these forces are sufficient to drive dislocation motion. Therefore, the deformation process can be interpreted as follows: the electric field induces surface atom evaporation, generating surface steps and edges that increase local roughness. These features have two primary effects: first, they slightly enhance the local electric-field stress, which scales with the square of the field strength (Supplementary Note 2); second, they act as classical stress concentrators, thereby lowering the barrier for dislocation nucleation. As steps and edges grow, their stress-concentration factors increase, eventually driving the local stress above the nucleation threshold[45]. Once near-surface dislocations form, the electron wind is sufficient to drive their propagation from the surface into the bulk, as particularly evident in the comparisons between Fig. 2 and Fig. 4. Furthermore, the combined action of the strong electric field and electron wind enhances surface atom migration and evaporation, and the electron wind promotes dislocation generation, motion, annihilation, and regeneration, thereby driving the evolution of electrode morphology. Notably, this work does not focus on tracking the nucleation and motion of an individual dislocation under high electric field, which likely occur within seconds or less. Instead, the collective evolution of dislocations (involving multiple dislocation nucleation, annihilation, and motion events) is examined during surface morphological changes, as this process occurs over a much longer timescale than that of a single dislocation event. Based on experimental observations, the dislocation nucleation process is largely surface-driven, involving roughness-enhanced electric field stress and its stress concentration effect[46], high surface atom free energy (especially at edges)[47], electron-wind-assisted surface atomic displacement[48], and stress redistribution due to surface atom evaporation. The dislocation annihilation process is primarily attributed to the high surface-to-volume ratio of nanotips, where free surfaces act as efficient sinks, and to the formation of dipoles by dislocations of opposite sign[49,50].

44. Zhao, S. T., Zhang, R. P., Chong, Y., Li, X. Q., Abu-Odeh, A., Rothchild, E., Chrzan, D. C., Asta, M., Morris, J. W., Minor, A. M. Defect reconfiguration in a Ti-Al alloy via electroplasticity. *Nat Mater* **20**, 468-472 (2021).
45. Anderson, P. M., Hirth, J. P., Lothe, J. Theory of dislocations (Cambridge University Press, 2017).
46. Gouldstone, A., Van Vliet, K. J., Suresh, S. Nanoindentation - Simulation of defect nucleation in a crystal. *Nature* **411**, 656-656 (2001).
47. Ding, R. K., Azadehranjbar, S., Espinosa, I. M. P., Martini, A., Jacobs, T. D. B. Separating Geometric and Diffusive Contributions to the Surface Nucleation of Dislocations in Nanoparticles. *ACS Nano* **18**, 4170-4179 (2024).
48. Li, X. Q., Turner, J., Bustillo, K., Minor, A. M. situ transmission electron microscopy investigation of electroplasticity in single crystal nickel. *Acta Mater* **223**, 117461 (2022).
49. Zhu, T., Li, J., Samanta, A., Leach, A., Gall, K. Temperature and strain-rate dependence of surface dislocation nucleation. *Phys Rev Lett* **100**, 025502 (2008).
50. Essmann, U., Mughrabi, H. Annihilation of dislocations during tensile and cyclic deformation and limits of dislocation densities. *Philos Mag A* **40**, 731-756 (1979).

5. The 5-minute observation intervals may be insufficient to fully capture dislocation nucleation. The authors should comment on how this temporal granularity affects the interpretation of their dynamic processes.

Response:

Thank you for your comment. We agree that 5-minute observation intervals may not fully resolve the rapid timescale of individual dislocation nucleation events, which likely occur within seconds or less. However, our study focuses on the collective evolution of dislocations (involving multiple dislocation nucleation, annihilation, and motion events) during surface morphological changes, a process that spans significantly longer timescales than single-event nucleation. Although the chosen temporal granularity may preclude direct observation of isolated nucleation events, it is adequate for resolving the progressive evolution of dislocation density and distribution during surface morphological changes. We have included this clarification in the revised manuscript:

Revised manuscript:

Lines 320-330:

Notably, this work does not focus on tracking the nucleation and motion of an individual dislocation under high electric field, which likely occur within seconds or less. Instead, the collective evolution of dislocations (involving multiple dislocation nucleation, annihilation, and motion events) is examined during surface morphological changes, as this process occurs over a much longer timescale than that of a single dislocation event. Based on experimental observations, the dislocation nucleation process is largely surface-driven, involving roughness-enhanced electric field stress and its stress concentration effect[46], high surface atom free energy (especially at edges)[47], electron-wind-assisted surface atomic displacement[48], and stress redistribution due to surface atom evaporation. The dislocation annihilation process is primarily attributed to the high surface-to-volume ratio of nanotips, where free surfaces act as efficient sinks, and to the formation of dipoles by dislocations of opposite sign[49,50].

6. Since the local electric field is geometry-dependent, do the authors account for changes in the enhancement factor as the tip shape evolves (especially between polyhedral and spherical stages)?

Response:

Thank you for your comment. We have included the electric field distribution for atomistic spherical and polyhedral nanotips with apex radii of 2 nm, 3 nm and 5 nm, a detailed explanation regarding this point is provided in our response to Comment 3.

7. The extrapolation to softer metals like copper and gold is interesting, but it would be more convincing if supported by literature citations or preliminary comparative data.

Response:

Thank you for the insightful comment. To support this extrapolation, we have added literature-reported surface self-diffusion barriers. Specifically, the diffusion barrier is 0.920 eV for a W atom on the close-packed W{110} surface [Ehrlich and Hudda, *J. Chem. Phys.* 44, 1039–1049 (1966);

Antczak and Ehrlich, Cambridge Univ. Press (2010)], while much lower values are reported for Cu/Cu{111} (0.036 eV) [Antczak and Ehrlich, Cambridge Univ. Press (2010); Ferrón et al., *Phys. Rev. Lett.* 93, 166107 (2004)] and Au/Au{111} (0.021 eV) [Liu et al., *Surf. Sci.* 253, 334–344 (1991); Antczak and Ehrlich, Cambridge Univ. Press (2010)]. These data indicate that copper and gold are considerably more susceptible to field-induced effects compared to tungsten.
We have modified this sentence in the revised manuscript:

Revised manuscript:

Lines 353-358:

It is worth mentioning that, although tungsten has relatively high surface diffusion barriers (0.920 eV for an adatom placed on the close-packed W{110} surface)[52, 53], clear deformation phenomena are still observed in our experiments. For metals with much lower diffusion barriers, such as Cu on Cu{111} (0.036 eV[53, 54]) and Au on Au{111} (0.021 eV[53, 55]), both corresponding to their close-packed surfaces, the field-induced effects are expected to be even stronger.

52. Ehrlich, G., Hudda, F. G. Atomic View of Surface Self-Diffusion - Tungsten on Tungsten. *J Chem Phys* **44**, 1039-1049 (1966).
53. Antczak, G., Ehrlich, G. Surface diffusion: metals, metal atoms, and clusters (Cambridge University Press, 2010).
54. Ferrón, J., Gómez, L., de Miguel, J. J., Miranda, R. Nonstochastic behavior of atomic surface diffusion on Cu(111) down to low temperatures. *Phys Rev Lett* **93**, 166107 (2004).
55. Liu, C. L., Cohen, J. M., Adams, J. B., Voter, A. F. Eam Study of Surface Self-Diffusion of Single Adatoms of Fcc Metals Ni, Cu, Al, Ag, Au, Pd, and Pt. *Surf Sci* **253**, 334-344 (1991).

8. Optional. Some elements in the Supplementary Information (e.g., the experimental setup in Suppl. Fig. 1b, simulations ruling out thermal effects) may be considered for insertion in the main text or figures for better clarity, if there is place.

Response:

Thank you for your comment. We have included the schematic of the experimental geometry in Figure 1.

Revised manuscript:

Lines 86-87:

Figure 1a-b shows the in situ electrically biased TEM holder and the schematic diagram of the experimental system.

Lines 130-139:

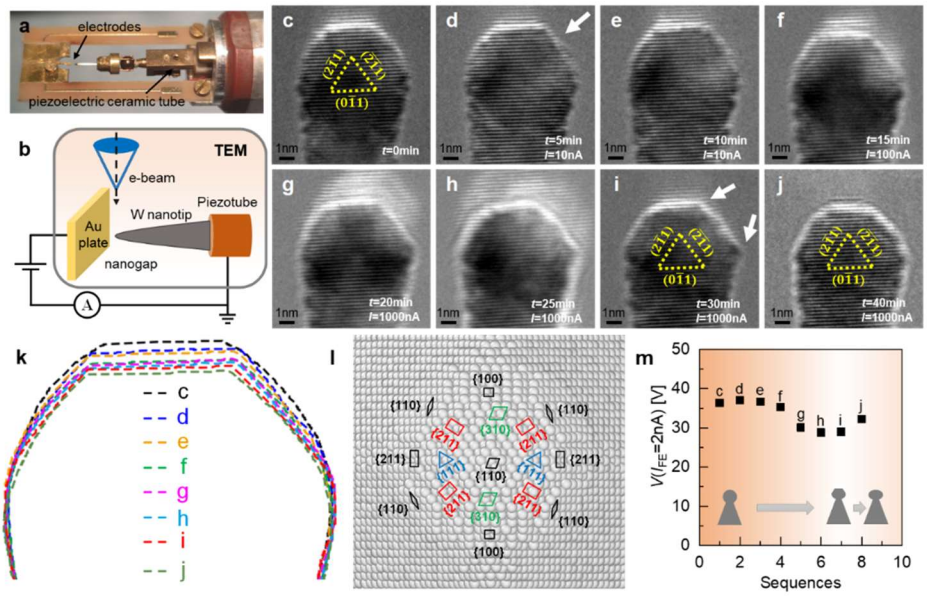

Fig. 1 a The in situ electrically biased TEM holder. **b** The schematic diagram of the in situ electrical measurement and micromorphology characterization system. **c-j** TEM images showing the progressive deformation behaviors of a <110>-oriented tungsten nanotip with an apex radius of 3 nm during field emission. The corresponding field emission current (I_{FE}) and the cumulative treatment time (t) are indicated in the lower right corner of each image. **k** The surface profiles of tungsten nanotips. **l** The top view of an atomistic model illustrating a <110>-oriented tungsten nanotip with an apex radius of 3 nm. **m** The applied voltages required to achieve a field emission current of 2 nA (d = 15 nm) is plotted in relation to the morphology changes of this tungsten nanotip.

Lines 461-462:

The morphology evolution experiment of pure tungsten nanotips is composed of two periods, the “treatment” period and the “observation” period, as shown in Supplementary Fig. 2.

Supplementary Information:

Lines 18-19:

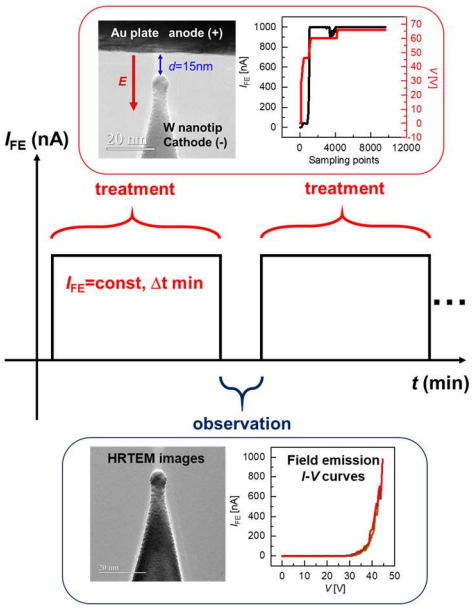

Supplementary Fig. 2| The experimental process for tracking deformation behaviors.

9. Minor edits are recommended for clarity and grammar (e.g., repeated use of "close-to-spherical", missing third person "s" in verbs, etc.) to enhance readability.

Response:

Thank you for your comment. We have revised the manuscript by changing some instances of "close-to-spherical" to "sphere-like", "nearly spherical" or "near spherical", and have corrected some grammatical errors.

REVIEWER COMMENTS

Report of Reviewer #1 -- NCOMMS-25-43028 by Yimeng Li et al

The authors of the paper 'Unveiling Electric-Field-Deformation Dynamics in Metal Nanostructures' have taken my suggestions for improvement on board and improved the text accordingly. There is still a problem with Figure 1, however: due to the addition of two images showing the experimental setup (which I think is very good), the slightly enlarged font size is still too small. I therefore ask the authors to ensure that the lettering is clearly legible.

I also believe that the suggestions made by the other reviewers have been well addressed and implemented.

Response:

We sincerely thank you for your positive comments. We are grateful for your constructive feedback throughout the review process, which has helped us significantly strengthen the manuscript.

I therefore recommend the acceptance of this very interesting paper, but please improve Figure 1 beforehand.

Response:

Thank you for your comment. We have revised Figure 1 by increasing the font size to ensure better readability, as shown below:

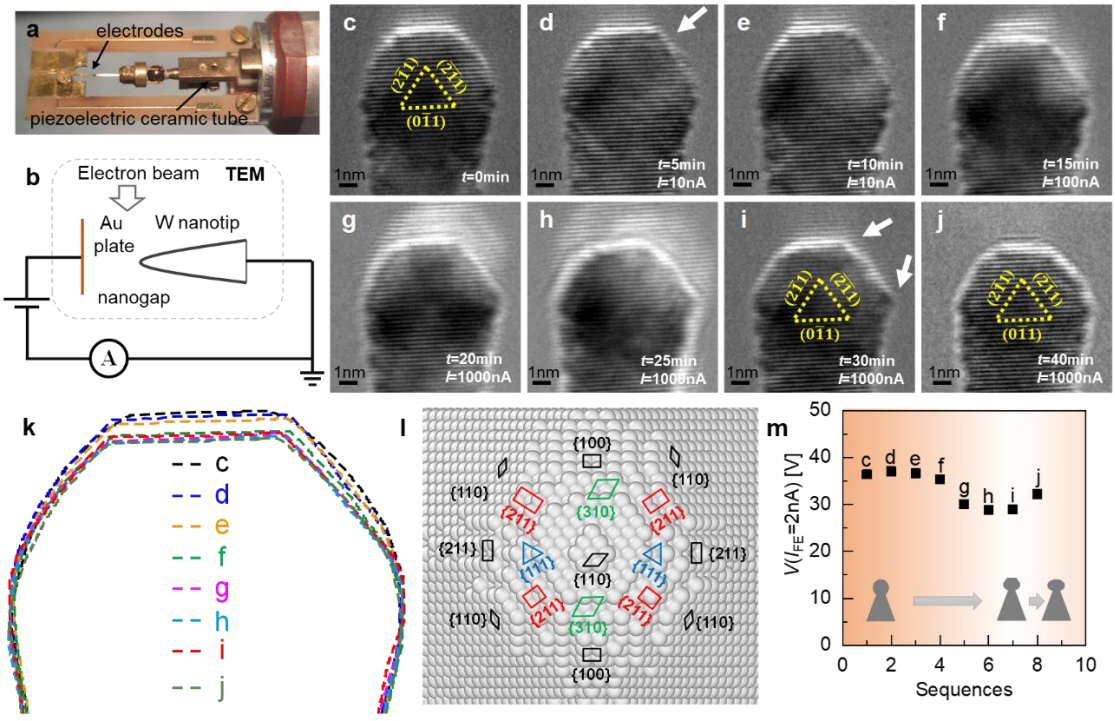

Report of Reviewer #2 -- NCOMMS-25-43028 by Yimeng Li et al

The authors have addressed all critical concerns in a satisfactory manner. I now support publication of this manuscript in its revised form.

Response:

We sincerely thank you for your positive comments. We are grateful for your constructive feedback throughout the review process, which has helped us significantly strengthen the manuscript.

Report of Reviewer #3 -- NCOMMS-25-43028 by Yimeng Li et al

In the revision, the authors have addressed the reviewer comments thoroughly, and the manuscript is now significantly improved in clarity, methodology, and depth of interpretation.

I appreciate the inclusion of multislice image simulations, which validate that the dislocation contrasts observed in the FFT-filtered HRTEM images are physically meaningful. The clarification and the discussion of possible resolution limits are transparent and scientifically honest. The authors also expanded the discussion on the evolution of the field enhancement factor, improved figure quality and annotation, and integrated data from the Supplementary Information into the main text. These changes enhance the manuscript's readability and coherence.

Overall, the revised version now presents a clear and compelling story supported by quantitative analysis and well-controlled in situ experiments.

I am satisfied that my previous comments, as well as those from the other reviewers, have been addressed.

I support publication of the manuscript in its present form.

Response:

We sincerely thank you for your positive comments. We are grateful for your constructive feedback throughout the review process, which has helped us significantly strengthen the manuscript.

Note: There is a minor typo in ref 56 in manuscript file and ref. 2 in Supporting Information. Please check.

Response:

Thank you for your comment. We have corrected the minor typos in ref. 56 in the manuscript and ref. 2 in the Supplementary Information.

Revised manuscript:

Lines 673-674:

56. Koch, C. T. Determination of core structure periodicity and point defect density along dislocations. Arizona State University (2002).

Supplementary Information:

Lines 239-240:

2. Koch, C. T. Determination of core structure periodicity and point defect density along dislocations. Arizona State University (2002).